Experimental Neurology 282 (2016) 99–118

Contents lists available at ScienceDirect

Experimental Neurology

journal homepage: www.elsevier.com/locate/yexnr

The novel KMO inhibitor CHDI-340246 leads to a restoration of electrophysiological alterations in mouse models of Huntington's disease

Vahri Beaumont [a], Ladislav Mrzljak [a], Ulrike Dijkman [b], Robert Freije [b], Mariette Heins [b], Arash Rassoulpour [b], Geoffrey Tombaugh [c], Simon Gelman [c], Amyaouch Bradaia [d], Esther Steidl [d], Melanie Gleyzes [d], Taneli Heikkinen [e], Kimmo Lehtimäki [e], Jukka Puoliväli [e], Outi Kontkanen [e], Robyn M. Javier [a], Ioana Neagoe [f], Heike Deisemann [f], Dirk Winkler [f], Andreas Ebneth [f], Vinod Khetarpal [a], Leticia Toledo-Sherman [a], Celia Dominguez [a], Larry C. Park [a], Ignacio Munoz-Sanjuan [a,*]

[a] CHDI Foundation/CHDI Management Inc., Los Angeles, USA
[b] Brains Online, San Francisco, USA
[c] Psychogenics, Montvale, USA
[d] Neuroservice SARL, Aix-en-Provence, France
[e] Charles River Discovery Services, Kuopio, Finland
[f] Evotec AG, Hamburg, Germany

ARTICLE INFO

Article history:
Received 3 December 2015
Received in revised form 28 April 2016
Accepted 5 May 2016
Available online 6 May 2016

Keywords:
Kynurenine
Kynurenic acid
Inhibitor
Huntington's disease
Quinolinic acid
Pharmacodynamic
Neurodegeneration
Q175
R6/2

ABSTRACT

Dysregulation of the kynurenine (Kyn) pathway has been associated with the progression of Huntington's disease (HD). In particular, elevated levels of the kynurenine metabolites 3-hydroxy kynurenine (3-OH-Kyn) and quinolinic acid (Quin), have been reported in the brains of HD patients as well as in rodent models of HD. The production of these metabolites is controlled by the activity of kynurenine mono-oxygenase (KMO), an enzyme which catalyzes the synthesis of 3-OH-Kyn from Kyn. In order to determine the role of KMO in the phenotype of mouse models of HD, we have developed a potent and selective KMO inhibitor termed CHDI-340246. We show that this compound, when administered orally to transgenic mouse models of HD, potently and dose-dependently modulates the Kyn pathway in peripheral tissues and in the central nervous system. The administration of CHDI-340246 leads to an inhibition of the formation of 3-OH-Kyn and Quin, and to an elevation of Kyn and Kynurenic acid (KynA) levels in brain tissues. We show that administration of CHDI-340246 or of Kyn and of KynA can restore several electrophysiological alterations in mouse models of HD, both acutely and after chronic administration. However, using a comprehensive panel of behavioral tests, we demonstrate that the chronic dosing of a selective KMO inhibitor does not significantly modify behavioral phenotypes or natural progression in mouse models of HD.

1. Introduction

The kynurenine (Kyn) pathway (KP) is the major catabolic pathway for the degradation of tryptophan, and several KP metabolites have important functions in the context of brain function and in the modulation of the immune system (Campbell et al., 2014; Maddison and Giorgini, 2015; Stone and Darlington, 2013). Kyn catabolism is mediated by multiple enzymes, which are differentially expressed in tissues and cell types. Kynurenine mono-oxygenase (KMO) catabolizes Kyn to generate 3-OH-kynurenine (3-OH-Kyn), which is subsequently catabolized to 3-OH-anthranilic acid (3-OH-AA) and quinolinic acid (Quin). Kynurenine is also converted to kynurenic acid (KynA) by a group of enzymes termed Kynurenine amino-transferases (KATs) with diverse distribution across tissues and species. Finally, kynureninase converts Kyn to anthranilic acid (AA), which can be further metabolized to generate 3-OH-AA (Fig. 1A). Several of the KP metabolites have been shown to be neuroactive and alterations in their levels has been associated with a variety of brain disorders, most notably in the context of neurodegeneration, cognition and affective disorders (Campbell et al., 2014; Maddison and Giorgini, 2015; Stone and Darlington, 2013). Adding further to the complexity of KP signaling, multiple KP metabolites can cross the BBB from the periphery via the action of amino acid transporters expressed in the brain vascular endothelium. This means that peripheral modulation of KMO activity can lead to an elevation in Kyn, which can access the brain and elevate KynA levels in the CNS via the activity of KATs expressed in astrocytes (Fukui et al., 1991; Heyes et al., 1997; Jauch et al., 1993).

Huntington's disease (HD) is a neurodegenerative disorder caused by a CAG trinucleotide repeat expansion in exon 1 of the *huntingtin*

* Corresponding author.
E-mail address: Ignacio.munoz@chdifoundation.org (I. Munoz-Sanjuan).

http://dx.doi.org/10.1016/j.expneurol.2016.05.005
0014-4886/

gene (*Htt*) (The Huntington's Disease Collaborative Research Group, 1993), leading most notably to a degeneration of the spiny projection neurons (SPNs) of the striatum (caudate-putamen) and widespread heterogeneous cortical regional atrophy, marked by a loss of layer II/III and deeper layer V and VI neurons (Waldvogel et al., 2015). The clinical phenotype of HD reflects to a large extent alterations in cortico-basal ganglia circuitry, leading to abnormal voluntary and involuntary movements, lack of motor coordination, postural defects, along with cognitive deficits and psychiatric symptoms (Cowan and Raymond, 2006; Ross et al., 2014).

The KP's involvement in HD has been well described. The activity of KMO has been reported to be increased in post-mortem HD brain samples and in animal models of HD (Forrest et al., 2010; Guidetti et al., 2006; Guidetti et al., 2004; Guidetti et al., 2000; Pearson and Reynolds, 1992; Sathyasaikumar et al., 2010), displaying regional increases in activity that appear to match the regional atrophy observed in disease (Beal et al., 1991; Campesan et al., 2011; Connick et al., 1988; Forrest et al., 2010; Guidetti et al., 2004; Guidetti et al., 2000; Pearson and Reynolds, 1992; Sathyasaikumar et al., 2010; Stoy et al., 2005). As 3-OH-Kyn and Quin are downstream metabolites of KMO activity in the KP pathway, the elevation of these metabolites in HD suggested they may contribute to some of the pathological and symptomatic hallmarks of HD. Quin in particular has been associated with HD pathology due to the observation that high concentrations of Quin can induce lesions reminiscent of HD in rodents and non-human primates (Beal et al., 1991; Ferrante et al., 1993). As in HD, these lesions are exemplified by the loss of SPNs in the striatum and the sparing of several interneuronal populations (Schwarcz et al., 2010). The mechanism by which Quin causes HD-like lesions in animals was proposed to be mediated by the agonistic activity of Quin on NMDA receptors and resulting excitotoxicity (Beal et al., 1991; Monaghan and Beaton, 1991). There have been several reports describing a paradoxical resistance of a few mouse models of HD to direct intra-striatal Quin administration, although these effects are not always conserved across models and the implications of these findings are unclear (Graham et al., 2009; Hansson et al., 2001; Hansson et al., 1999; Petersen et al., 2002). Quin elevations have also been correlated with neuroinflammatory conditions leading to extensive neuronal degeneration, such as those observed after HIV/SIV infection (Heyes et al., 2001; Valle et al., 2004). Additionally, the role of KMO activity in HD pathology extends beyond the elevated Quin hypothesis, as yeast and fly experiments also point to KMO as a critical enzyme in HD pathology (Campesan et al., 2011; Giorgini et al., 2013). Loss of activity, through either genetic deletion or pharmacological inhibition, reduced toxicity of mutant HTT (mHTT) fragments in these model systems, which do not generate Quin.

The conversion of Kyn to KynA by KAT enzymes can be further enhanced by the pharmacological blockade of KMO, with a resulting shift to KAT metabolism of Kyn. This increase in KynA has been postulated to be of benefit in HD through the potential antagonistic activity of KynA at the NMDA receptor. In support of this hypothesis a KynA analog showed beneficial effects in the N171-82Q fragment model of HD (Zadori et al., 2011). At high levels (μM), KynA inhibits NMDA receptors (Foster et al., 1992; Kessler et al., 1989), potentially opposing the actions of Quin and providing neuroprotective effects from excitotoxic stimuli (Connick et al., 1988). However, as with Quin elevation, the endogenous concentrations of KynA are in the nanomolar range, well below the concentrations needed to modulate NMDARs. Thus, whether this mechanism is at play at KynA levels induced by KMO inhibition is unclear. Other reports have suggested that KynA can modulate neurotransmitter (namely glutamate and dopamine) release *in vivo* when administered directly at submicromolar concentrations, possibly via the modulation of α7-containing nicotinic cholinergic receptors (α7-nAchR) (Albuquerque and Schwarcz, 2013; Banerjee et al., 2012; Beggiato et al., 2013; Wu et al., 2010). Additionally, both Kyn and KynA have been shown to have a vasodilatory effect at low physiological μM concentrations, which are observed in plasma, and which may affect brain function (Wang et al., 2010).

For HD, there are two major hypotheses associated with the dysregulation of the KP and KMO in particular. First, that the elevation of 3-OH-Kyn and Quin in HD models is sufficient to drive pathogenesis, and that decreasing their levels would be beneficial in the contexts of brain pathology and inflammatory mechanisms. Second, that the elevation of Kyn and KynA, on their own, would confer some benefit in HD models due to their neuroactive properties. We therefore developed an orally-bioavailable, potent and selective KMO inhibitor, CHDI-340246, to rigorously evaluate the involvement of KMO in disease progression (Toledo-Sherman et al., 2015; Winkler et al., 2013). We show a dose-dependent modulation of the KP metabolites in blood and in multiple tissues, including brain, after oral administration and provide a detailed quantitative pharmacokinetic-pharmacodynamic characterization of drug activity.

Lastly, we extensively characterize the effects of CHDI-340246 in two mouse models of HD, the R6/2 and the Q175 knock-in model (Heikkinen et al., 2012; Mangiarini et al., 1996; Menalled et al., 2012). We find that 3-OH Kyn and Quin levels in mice cannot be meaningfully lowered from already very low levels by KMO block. Therefore, the investigation of the neuro-inflammatory and excitotoxic hypotheses driven by high 3-OH-Kyn and Quin levels, at least using HD model mice, is not viable. In contrast, we did find neuroactive effects of Kyn and KynA when applied acutely, at concentrations physiologically achievable and mimicked through KMO inhibition. These include the rescue of several electrophysiological alterations found in hippocampal and cortico-striatal slice preparations obtained from HD models. Finally, the evaluation of chronic KMO inhibition in HD models revealed improvements in excitatory synaptic transmission in the striatum, but did not ameliorate disease progression.

2. Materials & methods

2.1. Selectivity assays for CHDI-340246 and KP metabolites

Selectivity of CHDI-340246 against KAT isoforms, kynureninase and IDO have been previously reported (referred to as compound 75 in (Toledo-Sherman et al., 2015; Winkler et al., 2013). In the present study, additional radioligand displacement assays with 10 μM CHDI-340246 were conducted against a diverse panel of CNS and other peripheral targets was performed to assess off-target liability (Cerep, France). See Table S1a, S1b.

To assess the activity of KP metabolites Kyn, 3-OH-AA, KynA, AA, 3-OH-Kyn and Quin against previously literature-reported putative targets, antagonist and agonist displacement radioligand studies were performed with endogenous NMDA, AMPA, kainate, and GABA receptors in rat cerebral cortex preparations, against endogenous α7 and α4β2 nicotinic acetylcholine receptors in SH-SY5Y cells, and with human $GABA_{A1}$ (α1β2γ2) receptors in CHO cells. See Table S5. Experimental conditions for each assay can be found on the provider webpage (www.cerep.fr).

2.2. Pharmacokinetic analysis of CHDI-340246 in mice

Dosing and tissue collection was conducted at Xenometrix (Switzerland). Bioanalysis of tissue and plasma samples was conducted at Tandem laboratories (North Carolina). Male C57BL/6N mice (Hilltop Laboratories; Scottsdale, PA) were individually housed and acclimated to the study room environment for 9 days prior to dose administration. Animals had access to food (LabDiet® Certified Rodent Diet 5002 Meal) and water *ad libitum*.

For the IV dose formulation, CHDI-340246 was dissolved via vortexing, stirring and gentle sonication in DMSO:PEG400:water (10:40:50 *v*/v/v) to a final concentration of nominal 1 mg eq. parent/mL, filtered into a sterile vial using a 0.2 μm Millex GV PVDF filter

(Millipore), and stored at 22 °C ± 5 °C, protected from light, until dosing. Subsequent bioanalysis of the resultant formulation indicated that a 1.0 mg eq/mL formulation was accurately achieved. Animals undergoing IV dosing were injected via tail vein at a dose volume of 5 mL/kg, for a 5 mg eq./kg dose.

For the PO dose formulation, CHDI-340246 was prepared as nominal 1 mg eq. parent/mL in 10% HPβCD in water *w/v* via gentle vortexing, sonicating, and stirring at room temperature. This formulation provided a clear liquid solution, and was stored at 22 °C ± 5 °C and protected from light until dosing. Animals undergoing PO dosing were given a 10 mL/kg volume via oral gavage, for a nominal 10 mg eq./kg dose. Subsequent bioanalysis of the resultant formulation indicated that the actual measured concentration was slightly higher than nominal at 1.35 mg eq/mL formulation. Actual dose level administered was thus adjusted to 14 mg eq./kg for subsequent relevant PK parameter value determination.

Plasma and tissue samples (brain, kidney and liver) for both iv and po dose routes were collected pre-dose, and at 0.083, 0.25, 0.5, 1, 2, 4, 8, 12, 24 h post dosing. n = 3 mice were used for each route of administration and each timepoint evaluated.

Concentrations of CHDI-340246 in mouse plasma, brain, kidney, liver, and dose solutions were determined using an LC-MS/MS assay as described previously (Toledo-Sherman et al., 2015). The lower limits of quantification (LLOQ) for this assay were 3.44 nM (plasma, kidney and liver) and 6.88 nM (brain).

Non-compartmental pharmacokinetic analyses of the plasma concentration time course were performed using WinNonlin, version 6.1 (Pharsight Corp., Mountain View, California).

2.3. Slice electrophysiological studies

2.3.1. Hippocampal electrophysiology

Electrophysiology was conducted at Neuroservice SARL (Aix-en-Provence, France). Experiments were performed with R6/2 CAG 120s (C57Bl/6) and age-matched WT mice at 8 weeks of age (Jackson Laboratory, Bar Harbor, USA).

Multielectrode array recordings were performed as described previously (Beaumont et al., 2014). In brief, field EPSPs were recorded following CA3 stimulation and recorded from CA1 stratum radiatum and stratum pyrimidale layers. Basal fEPSPs were recorded at 0.03 Hz for construction of input-output curves. Paired pulse ratio was recorded as the ratio of the second to first EPSC amplitude (inter-stimulus interval of 25 ms–300 ms). To evaluate compound effects, I—O and PPR was first recorded in the absence of compound, and then repeated in the presence of compound following compound administration for 20 min prior. For measurement of long term potentiation (LTP), basal fEPSPs were recorded at 0.03 Hz for 10 min at 40% of maximal fEPSP amplitude. LTP was induced by a theta burst induction paradigm (TBS) consisting of a single train of 10 bursts composed each of 4 stimuli at 100 Hz, applied with a 200 ms interval. Potentiation of fEPSP amplitude was then monitored for an additional 60 min period. In the case of treated slices, the whole LTP recording session was performed in the presence of a compound (final DMSO concentration of 0.1% DMSO) applied for 20 min prior to TBS, and compared to slices perfused with ACSF containing only 0.1% DMSO vehicle perfused for a similar amount of time. A minimum of 3 mice (range 3–8) per condition evaluated were used, with a minimum of 9 slices (range 9–47) collected per condition. Only if a compound showed effects in R6/2 slices, was it then progressed to testing in WT slices.

2.3.2. Striatal electrophysiology

270–300 μm thick para-horizontal corticostriatal brain slices from mixed gender 7–8 week old R6/2 and WT mice, or 6–7 month old Q175 wild-type or heterozygous KI mice were acutely prepared and recorded from as previously described (Heikkinen et al., 2012). We used two methods of drug evaluation. First, we examined the effect of compounds on neuronal and synaptic properties following acute application of compounds directly to the slices. SPN resting membrane potential (Vm/Vh), membrane resistance (Rm) Membrane current (Im), and rheobase in R6/2 and Q175, and evoked corticostriatal transmission (input-output curves (I—O) in R6/2 slices were first recorded in ACSF alone, and then subsequently following 15–30 min of CHDI-340246/KP metabolite application. Membrane resistance was determined from a + 5 mV step from Vh of −80 mV, unless noted. Drugs were diluted into the bath solution immediately before use. A fresh (drug-naïve) slice was used for each experimental trial. For experiments employing preincubation of slices with the guanylyl cyclase inhibitor ODQ (10 μM), the adenylyl cyclase inhibitor SQ 22536 (10 μM), and the PKG inhibitor KT5283 (1 μM), inhibitors were added to slices for a minimum period of 1 h during recovery following slicing in the holding chamber. SQ 22536 and ODQ were then perfused at 10 μM throughout the subsequent recording period, whereas KT5832 was perfused at 0.5 μM throughout the recording period.

In an alternate format, we dosed 4 week old R6/2 and WT littermate mice for 4–8 weeks po bid *in vivo*; and 2 month old Q175 heterozygous and WT mice for 4 months po bid *in vivo*, with CHDI-340246 or vehicle alone. CHDI-340246 was formulated in 10% (*w/v*) hydroxypropyl-β-cyclodextrin (HP-β-CD) in 50 mM citrate buffer (pH 5.5). R6/2 dosing and electrophysiological recording was performed at Psychogenics (USA). Q175 dosing was performed at Charles River (Finland), and animals were shipped to Neuroservice SARL (France) for recording. Sacrifice of animals and preparation of slices occurred within 24–72 h post-last dose (R6/2) or between 72 h–2 weeks post last dose (Q175). In this scenario, CHDI-340246 was absent during the recording period, and any improvement in synaptic and neuronal parameters in the HD recordings could be ascribed to a sustained improvement in synaptic or SPN function which arose from the prior chronic dosing regimen. Experimenters were blinded to both the genotype of the mice and the dosing previously undertaken until analysis was completed. SPN Vm, Rm and rheobase (R6/2 and Q175) were recorded as described. To record miniature excitatory postsynaptic currents (mEPSCs), the standard K^+ gluconate based intracellular solution was replaced with a Cs-methanesulfonate based solution, and all recordings were performed at Vh = −80 mV with the addition of tetrodotoxin (TTX, 0.5 μM) and picrotoxin (30–40 μM) to the ACSF, as previously described (Heikkinen et al., 2012).

2.3.3. Data analysis

Data were analyzed with Clampfit 10 (Molecular Devices) and Prism 6 (GraphPad). mEPSCs recordings were analyzed for amplitude and frequency using Minianalysis (Synaptosoft). After the automatic detection of events, each trace was manually corrected for false positives and false negatives. Results from evaluation of membrane properties and mEPSC parameters are presented as box and whisker plots, where the box indicates the 25–75th percentile, the median is represented by the line, and whiskers represent the 10–90% range. Outlier values are indicated as individual data points. Mean values are indicated by +. For input-output (I—O) curves and cumulative probability curves, mean ± sem values are shown. For normalization of the I—O curves, the maximum achievable averaged eEPSC amplitude per neuron recorded (or averaged max fEPSP amplitude per slice for hippocampal recordings), regardless of stimulus intensity required to achieve this, was assigned a value of 1, and all other eEPSC/fEPSP amplitudes recorded from that neuron/slice at varying stimulus intensities are presented as the fraction of that value. Statistical analysis was performed via Mann-Whitney *t*-test, Ordinary or Repeat Measures ANOVA with multiple comparison correction, as appropriate, and described further in results. For statistical evaluation of hippocampal LTP, statistics were performed on data points 20–60 min post-TBS induction, after the post-tetanic potentiation phase had diminished.

2.4. Cell culture electrophysiological studies monitoring effects of KP metabolites on NMDA receptor and nicotinic α7-subunit acetylcholine (α7nAch) receptor currents

HEK293 cells were transiently transfected with EGFP, NR1 + NR2A or NR1 + NR2B in 1:1.5:0.25 ratio for NR1: NR2A: EGFP or 1:0.8:0.25 for NR1: NR2B: EGFP. After transfection (Fugene, Roche Applied Bioscience), cells were kept at 37 °C in DMEM/F12 medium (Cell Culture Technologies), supplemented with L-glutamine (2 mM) and the NMDA receptor antagonists D-AP5 (50 μM) and ketamine (500 μM). The cells were used 48h after transfection. To achieve functional expression of human α7 nAChR in HEK293 cells, cells were tranfected with human α7 nAChR co-expressed with ric-3 and GFP in a 1:1:0.4 ratio (Williams et al., 2005). The cells were maintained in DMEM Mix Medium (Sigma) 24-48 h prior recording.

Transiently transfected HEK 293 cells were superfused with an external solution containing (in mM): 130 NaCl, 5.4 KCl, 2 $CaCl_2$, 10 HEPES, 5 glucose, pH = 7.4 at room temperature. Patch pipettes were filled with an intracellular solution which contained (in mM): 140 KCl, 0.5 $CaCl_2$, 10 HEPES, 11 EGTA, 2 NaATP, pH = 7.2. Membrane currents were recorded from a holding potential of −60 mV using an EPC10 amplifier and Pulse software (HEKA). Glu/Gly/Ach and the KP metabolites were applied via Dynaflow, a fast exchange perfusion system (Cellectricon, Sweden). The agonist-evoked currents were analyzed using Pulse (HEKA software) and Excel (Microsoft software).

Glutamate, glycine and Quin were dissolved in water, whereas stock solutions of all the other metabolites were prepared in DMSO, for a final DMSO concentration of 1% during recording. As 1–5% DMSO has been shown previously to inhibit α7 nAchR currents (Mok et al., 2009) in a α7 nAchR-containing GH4 cell line, we evaluated 1% DMSO alone and could not detect any current inhibition.

2.5. In vivo pharmacodynamic and efficacy studies in mice with CHDI-340246

For all *in vivo* studies, CHDI-340246 was formulated in 10% (*w*/*v*) hydroxypropyl-β-cyclodextrin (HP-β-CD) in 50 mM citrate buffer (pH 5.5 ± 0.2) in reverse osmosis water for oral administration (po).

2.6. Microdialysis studies in mice

Experiments were performed at Brains On-Line LLC (South San Francisco, CA, USA).

Male Q175 hets and wildtype mice aged 22–23 weeks (CHDI-81003003, CHDI) were used for the experiments. Prior to experimentation, the animals were group housed in plastic cages and had access to food and water *ad libitum*. Experiments were conducted in accordance with the declarations of Helsinki and were approved by the Institutional Animal Care and Use Committee.

Mice were anesthetized using isoflurane (2%, 800 mL/min O_2). Bupivacain/epinephrine was used for local analgesia. Fynadine was used for peri−/post-operative analgesia. The animals were placed in a stereotaxic frame (Kopf instruments, USA) and either I-shaped microdialysis probes for pharmacodynamics assessment, or metaquant (MQ) probes for pharmacokinetic measurements, were inserted into the striatum. Coordinates for the tips of the probes were for the striatum: posterior (AP) = +0.8 mm to bregma, lateral (L) = −1.7 mm to midline and ventral (V) = −4.0 mm to dura, the toothbar was set at 0.0 mm. After surgery, animals were kept individually in cages, and afforded food and water *ad libitum*.

Experiments were performed one day after surgery. The probes of the animals were connected with flexible PEEK tubing to a microperfusion pump (Harvard PHD 2000 Syringe pump, Holliston, MA or similar). I-shaped microdialysis probes were perfused with aCSF containing 147 mM NaCl, 3.0 mM KCl, 1.2 mM $CaCl_2$ and 1.2 mM $MgCl_2$, at a flow rate of 1.5 μL/min. MQ microdialysis probes were perfused with aCSF containing 147 mM NaCl, 3.0 mM KCl, 1.2 mM $CaCl_2$ and 1.2 mM $MgCl_2$, at a flow rate of 0.15 μL/min, with a carrier flow of ultrapure water at 0.8 μL/min.

I-shaped microdialysis samples (30 μL) were collected in 20-min intervals by an automated fraction collector (820 Microsampler, Univentor, Malta) into mini-vials already containing 10 μL 0.02 M formic acid (FA) + 0.04% ascorbic acid in ultrapurified H_2O. The total nominal sample volume was 40 μL. Six basal samples were collected. At $t = 0$ min, vehicle or 10 mg/kg CHDI-340246 was administered po. Sample collection was continued for $t = 240$ min after compound administration. MQ microdialysis samples (19 μL) were collected in 20-min intervals by an automated fraction collector (820 Microsampler, Univentor, Malta). At $t = 0$ min, vehicle or CHDI-340246 was administered po. After the experiment, the mice were sacrificed and terminal plasma (Na-heparin treated), CSF, brain, liver, kidney and tail tip samples were taken.

All microdialysis samples were stored at −80 °C awaiting their analysis. The brain samples were split in two hemispheres: one was used to verify the probe position, and the other hemisphere was stored at −80 °C and used for bioanalysis of KP metabolites.

For preparation of LC-MS samples from plasma samples, an aliquot of internal standard solution was mixed with an aliquot of each plasma sample. The mixture was centrifuged and the supernatant was transferred to a vial suitable for use in the autosampler. For extraction of the analytes from tissue matrix, extraction solvent, consisting of 0.01% ascorbic acid and 50% acetonitrile in ultrapurified H_2O, was added to each sample at a volume of 4 mL/g. The sample was homogenized by sonication and the homogenate was centrifuged. The supernatant was used as tissue extract for quantification of kynurenine pathway metabolites.

Concentrations of Kyn, KynA, 3-OH-Kyn and AA were determined by HPLC with tandem mass spectrometry (MS/MS) detection using D4-Kyn, D5-KynA and D4-AA as internal standards (IS). Samples were injected onto the HPLC column by an automated sample injector (SIL20-AD, Shimadzu, Japan or similar). Chromatographic separation was performed on a Hypersil C18 analytical column (150 × 2.1 mm, particle size: 3 μm; Thermo) held at 25 °C. The mobile phases consisted of A: ultrapurified water with 0.1% formic acid and B: acetonitrile with 0.1% formic acid. Elution of the compounds was performed using a linear gradient at a flow rate of 0.2 mL/min.

Concentrations of Quin were determined by HPLC with tandem mass spectrometry (MS/MS) detection using D3-Quin as internal standard. Chromatographic separation was performed on a Synergi RP column (Phenomenex) held at 25 °C. The mobile phases consisted of A: ultrapurified water +0.2% acid and B: acetonitrile +0.2% acid. Elution of the compounds proceeded using a suitable linear gradient at a flow rate of 0.2 mL/min.

Recovery values through the microdialysis probes were as follows: Kyn (21.4%), KynA (18.0%), 3-OH-Kyn (28.8%), AA (27.8%), and Quin (18.3%).

The MS analyses were performed using an API 4000 MS/MS system consisting of an API 4000 MS/MS detector and a Turbo Ion Spray interface (Applied Biosystems, the Netherlands). The acquisitions on API 4000 were performed in positive ionization mode, with optimized settings for the analytes. The instrument was operated in multiple-reaction-monitoring (MRM) mode. Data were calibrated and quantified using the Analyst™ data system (Applied Biosystems).

2.7. Measurement of KMO activity

KMO activity determination was performed using mitochondrial fractions isolated from mouse brain tissue homogenates, essentially as described (Winkler et al., 2013).

2.8. Behavioral and brain volumetric studies in HD mouse models

All studies were conducted at Charles River Discovery Services, Kuopio, Finland. All animal experiments were conducted according to the National Institute of Health (NIH) guidelines for the care and use of laboratory animals, and authorized in Finland by the national Animal Experiment Board. Mice were kept housed as described previously (Beaumont et al., 2014; Heikkinen et al., 2012; Menalled et al., 2012).

Open field testing, rearing-climbing testing, rotarod testing, grip strength testing and in vivo MRI volumetry and MRS studies were conducted as previously reported (Beaumont et al., 2014; Heikkinen et al., 2012; Menalled et al., 2012).

Genotyping and CAG repeat count for Q175 hets and homs were determined by Laragen Inc. (Culver City, CA, USA) at 10–15 days of age by PCR of tail snips. The average CAG repeat length was 178.3 (range 173 to 182) in Q175 hets and 186.9 (range 174 to 200) in the Q175 homs. Genotyping and CAG repeat count for R6/2 mice were performed by PCR, and the average CAG repeat length was 125 (range 117 to 135).

Statistical analyses were performed using IBM SPSS Statistics 19 and StatsDirect software unless otherwise specified. Behavioral and MRI measures were analyzed with Linear Mixed Models, analyzing the interactions for genotype, age and genotype × age interaction. If significant genotype effect was found One-way ANOVA followed by Dunnett's post-hoc test (comparison to wild-type mice) was used for each time point separately. The MRS data were analyzed with One-way ANOVA for each time point and metabolite separately.

All values are presented as mean ± standard error of the mean (SEM), and differences are considered to be statistically significant at the $p < 0.05$ level.

2.9. Drugs

Kynurenine metabolites, glutamate, glycine and acetylcholine were procured from Sigma. CHDI-340246, UPF-648 and Ro-61-8048 were synthesized at Evotec (UK). 8-Br-cGMP, 1*H*-[1,2,4]Oxadiazolo[4.3-*a*]quinoxalin-1-one (ODQ), 9-(Tetrahydro-2-furanyl)-9*H*-purin-6-amine (SQ 22536) and KT5283 were procured from Tocris.

3. Results

CHDI-340246 is a novel, selective KMO inhibitor developed for the treatment of Huntington's disease. Its properties have been described previously, as compound 75 (Toledo-Sherman et al., 2015). In biochemical assays against KMO using mitochondrial fractions isolated from rodent liver tissue, CHDI-340246 has an IC_{50} of 0.5 nM. In various cellular assays measuring endogenous KMO activity, including primary rat microglia and human peripheral blood cells (PBMCs), and in CHO cells overexpressing mouse, human or rat KMO, CHDI-340246 has a potency

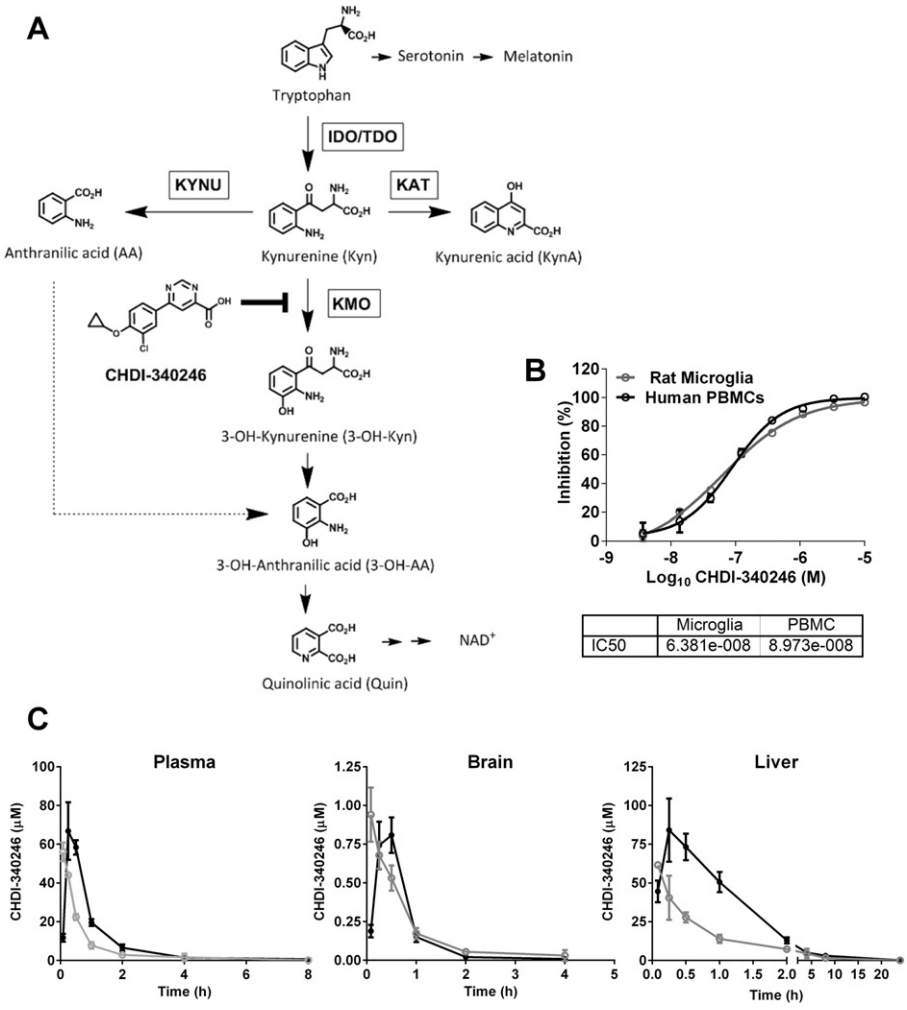

Fig. 1. Activity and pharmacokinetic properties of the KMO inhibitor CHDI-340246 in mice. (A) Kynurenine pathway diagram and structure of CHDI-340246. (B) Dose-response curves for CHDI-340246 in primary rat microglia and human PBMCs. (C) Pharmacokinetic analysis of CHDI-340246 dosed orally (po, 5 mg/kg, closed black circles) or intravenously (iv, 14 mg/kg, open grey circles) to mice.

of 20–80 nM, depending on the assay format [Fig. 1 and (Toledo-Sherman et al., 2015)]. CHDI-340246 does not affect the activity of other enzymes in the KP, including IDO, KATs or kynureninase. CHDI-340246 was selective for KMO when profiled against a diverse panel of central nervous system (CNS) and peripheral targets, as well as a diverse set of kinases and other representative sets of enzyme classes (Tables S1a and b).

3.1. Pharmacokinetic (PK) analysis of CHDI-340246 in mice

The PK analysis of CHDI-340246 in rats was previously reported (Toledo-Sherman et al., 2015). As mice are the major preclinical species of choice for HD research, we conducted PK and pharmacodynamic (PD) studies of CHDI-340246 in mice. Plots of the mean ± SD CHDI-340246 concentration in plasma, brain, and liver following a 5 mg/kg intravenous (IV) or 14 mg/kg po dose are shown in Fig. 1. A summary of the PK parameters in plasma, brain, kidney and liver is shown in Table 1, and mean tissue to plasma ratios are shown in Table 2.

The IV pharmacokinetics of CHDI-340246 in plasma was characterized by a low clearance (0.4 L/h/kg) and a low volume of distribution at steady state (0.44 L/Kg), and a half-life of 1.4 h. Following an oral dose, the compound was rapidly and relatively well absorbed, with a plasma C_{max} of 67 μM observed at 0.25 h, and an oral bioavailability (F %) of 60%. The distribution of CHDI-340246 to brain was very limited (ratio of 0.024 at Cmax (0.81 μM); 30 min post oral dose; Table 2). CHDI-340246 showed good distribution to kidney and liver (tissue: plasma ratios of 5.9 and 1.2, respectively, 30 min post oral dose; Table 2). In addition to brain, we measured kidney and liver levels, as these tissues have high expression of KMO. Kidney-to-plasma and liver-to-plasma ratios increased over time. These results are similar to those reported for rats (Toledo-Sherman et al., 2015).

Plasma protein binding studies showed CHDI-340246 to be highly bound (F_u 0.08 mouse). It is not known whether measurements of free or total tissue levels of CHDI-340246 achieved in the brain are more relevant to KMO inhibition in CNS. Therefore, we measured CHDI-340246 using quantitative (Metaquant, MQ) microdialysis probes implanted in the striatum, in order to determine the levels of unbound CHDI-340246 in the interstitial striatal space following systemic administration. At 10 mg/kg, the free concentration of CHDI-340246 ranged from 20 to 50 nM (close to the cellular IC_{50} of the enzyme for rat microglial KMO activity). We conducted more extensive studies at doses ranging from 30 to 100 mg/kg in WT and Q175 hets (n = 6 animals/group). The results from these studies are shown in Fig. S3. Using the dosed Q175 hets group values for this study, at 30 mg/kg po, the concentration of free striatal CHDI-340246 was 55 ± 33 nM (Cmax ± sem values), at 60 mg/kg it was 81 ± 42 nM, and at 100 mg/kg it reached 206 nM ± 150 nM in the extracellular space.

Table 1
Summary of pharmacokinetic parameters in plasma and brain following an intravenous (iv) or oral dose (po) of CHDI-340246 to fed male C57Bl/6 mice.

PK parameters	Units	Dose regimen: 5 mg eq./kg single iv bolus			
		Plasma	Brain	Kidney	Liver
$AUC_{(0\text{-}last)}$	nM h	43,000	700	250,000	78,000
$AUC_{(0\text{-}inf)}$	nM h	43,000	740	250,000	78,000
AUCN	nM h kg/mg	8600	150	50,000	16,000
Observed C_{max}	nM	NA	940	140,000	62,000
Observed $C_{max}N$	nM kg/mg	NA	190	28,000	12,000
Observed T_{max}	hr	NA	0.083	0.25	0.083
CL	L/h/kg	0.40	NA	NA	NA
MRT	h	1.1	NA	NA	NA
V_{dss}	L/kg	0.44	NA	NA	NA
Half-life ($t_{½}$)	h	1.4	0.84	2.9	2.9
Half-life regression time points	h	1, 2, 4, 8	0.25, 0.5, 1, 2, 4	2, 4, 8, 24	2, 4, 8, 24
PK parameters	**Units**	**Dose regimen: 14 mg eq./kg single po dose**			
		Plasma	**Brain**	**Kidney**	**Liver**
$AUC_{(0\text{-}last)}$	nM h	73,000	1100	370,000	160,000
$AUC_{(0\text{-}inf)}$	nM h	73,000	1100	370,000	160,000
AUCN	nM h kg/mg	5200	81	26,000	11,000
F	%	60	NA	NA	NA
Observed C_{max}	nM	67,000	810	200,000	84,000
Observed $C_{max}N$	nM kg/mg	4800	58	15,000	6000
Observed T_{max}	h	0.25	0.5	0.25	0.25
Half-life ($t_{½}$)	h	3.2	1.1	3.6	3.8
Half-life regression time points	h	4, 8, 24	0.5, 1, 2, 4, 8	4, 8, 24	4, 8, 24

NA: Not applicable pharmacokinetic parameters due to matrix or route of exposure.

Table 2
Tissue: plasma concentration ratios following an IV dose of CHDI-340246 to fed male C57Bl/6 mice.

Time point (h)	Brain: plasma		Kidney: plasma		Liver: plasma	
	Mean	SD	Mean	SD	Mean	SD
0.083	0.017	0.004	2.5	1.1	1.1	0.1
0.25	0.015	0.002	3.1	0.4	0.91	0.29
0.5	0.024	0.005	5.9	0.9	1.2	0.2
1	0.023	0.003	8.3	1.1	1.8	0.2
2	0.019	0.002	8.4	1.0	2.6	0.3
4	0.020	0.002	9.2	0.7	4.3	1.9
8	NC	NC	15	NC	9.3	NC
24	NC	NC	NC	NC	NC	NC

NC: Not calculated.
Mean was calculated when at least two concentration ratios were available.
SD was calculated when at least three concentration ratios were available.

3.2. Pharmacodynamic effects on KP metabolites in response to acute KMO inhibition in mice

In order to evaluate the biological effects of CHDI-340246 in mice, we evaluated plasma, brain tissue and extracellular levels of KP metabolites in selected brain regions. Extracellular levels of metabolites in striatal interstitial fluid were measured using I-shaped microdialysis probes implanted in the striatum of either wildtype (WT) or Q175 heterozygote (hets) mice, a knock-in model of HD (Heikkinen et al., 2012; Menalled et al., 2012).

Baseline levels were determined and shown not to be significantly different in 2–3 month old Q175 hets, with the exception of Quin levels, found to be mildly elevated (Table S2a). In spite of not detecting an increase in 3-OH-Kyn, we did confirm that enzymatic activity of KMO in tissue homogenates was elevated (2-fold) in Q175 hets at 6 months of age (Fig. S1).

Following po administration of 10 mg/kg CHDI-340246, a significant time-dependent elevation of extracellular Kyn, KynA and AA levels in the striatum of WT and Q175 hets was seen (n = 6–8 animals/group; Fig. 2). Kyn levels increased from approximately 5 nM in vehicle treated samples (mean levels provided), to 75–110 nM at Tmax; KynA levels increase from a baseline level of 0.25 nM to 14–19 nM; and AA levels increased from 1.5–1.7 nM baseline to 14–19.5 nM after CHDI-340246 dosing. In contrast, the levels of 3-OH-Kyn and Quin were changed little at this dose, from a baseline level of 3-OH-Kyn of 0.6–0.7 nM to 1.6–1.7 nM (approximately a 2–2.5 fold increase over baseline), and 1.5-fold increase in Quin levels (not shown).

The CNS Kyn elevation following KMO block results as a consequence of both peripheral and possibly CNS KMO block, as Kyn can readily cross the BBB. Following CHDI-340246 administration, flux through the KMO pathway (3-OH-Kyn/Kyn ratio) was reduced to 22 ± 2% of baseline flux in WT and 16 ± 2% of baseline flux in Q175, measured 100–240 min post-dose. In contrast, flux through the KAT catabolic route as measured by the KynA/Kyn ratio was rapidly enhanced ~4–5 fold 40 min post-dose, with a sustained increase in KynA/Kyn ratio ~ 2.5 fold measured 100–240 min post-dose. Catabolism of Kyn

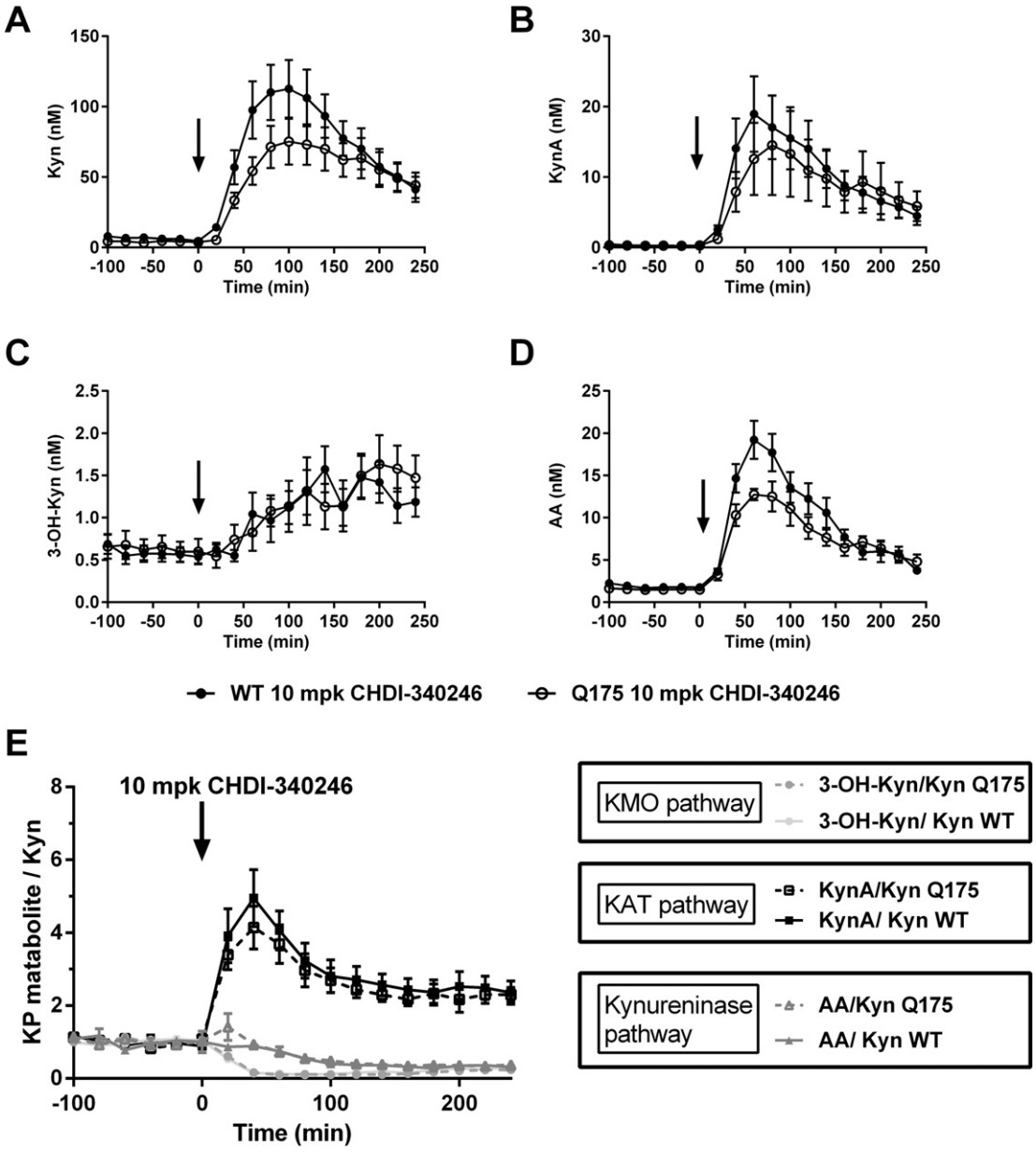

Fig. 2. Pharmacodynamic effects of orally administered CHDI-340246 on extracellular levels of kynurenine pathway metabolites in wildtype and Q175 hets. Microdialysis probes were implanted into the striatum of either WT (closed circles) or Q175 hets (open circles) at 6 months of age. An oral dose of CHDI-340246 was administered via oral gavage (arrow) and fractions were collected every 20 min through the microdialysis probes. Levels of KP metabolites were determined by LC-MS/MS and corrected for recovery through the probes. Values shown are corrected values. (A) Kyn levels; (B) KynA levels; (C) 3-OH-Kyn levels; (D) AA levels; (E) Flux through the pathways expressed as a ratio of KP metabolite/Kyn based on corrected concentrations normalized to baseline flux.

occurring through the kynureninase arm (AA/Kyn) was less favored. Thus, following KMO block by CHDI-340246, Kyn is catabolized primarily through KAT, producing KynA, which takes precedence over the kynureninase route of catabolism.

We also measured tissue homogenate levels of KP metabolites at a single time point ($t = 4$ h) after the microdialysis experiments were completed. The results show modulation of KP levels in brain, liver, and kidney as well as in plasma (Fig. S2). Generally, the response was a dose-dependent elevation of Kyn, AA and KynA in all tissues and plasma. For 3-OH-Kyn, kidney and liver levels decrease after dosing, although we failed to detect a significant effect in plasma at this dose and timepoint. In contrast, in the brain we observe a small increase in 3-OH-Kyn and Quin levels, consistent with the microdialysis study.

We further investigated the effects of higher doses of orally administered CHDI-340246 up to 100 mg/kg on CNS KP metabolite generation (Fig. S3). For Kyn, and KynA, AUC values were higher in 60 and 100 mg/kg treated animals than in 30 mg/kg treated animals. These larger AUC values at 60 and 100 mg/kg appear to be likely driven by the longer exposure of CHDI-340246 at these doses, resulting in sustained Kyn elevation, while Kyn and KynA peak (Cmax) values show saturation at doses higher than 30 mg/kg in mice after a single dose of CHDI-340246 (Fig. S3). KP metabolite levels showed the same general pattern as with the 10 mg/kg dose of CHDI-340246, with fold elevation in KynA and AA much higher than that seen in 3-OH-Kyn and Quin levels.

Interestingly, some differences in the absolute levels of KP metabolites generated following CHDI-340246 administration were noted between WT and Q175 mice. At 10 mg/kg CHDI-340246, the total elevation of Kyn as measured by the area under the curve (AUC) showed that while robust, the values were lower in Q175 compared to WT (2-way ANOVA [$F(1.45) = 4.969$, $p = 0.031$]), whereas there was

no statistically significant difference in the AUC for KynA or AA ($p = 0.177$ and $p = 0.324$, respectively). AUC values were also higher for Kyn in the 30, 60 and 100 mg/kg treated animals in WT compared to Q175 hets, showing this to be a conserved finding. A survey of tissue levels of KP metabolites among peripheral tissues and plasma 4 h following the 10 mg/kg dose of CHDI-340246 (Fig. S2) showed that liver Kyn levels were significantly higher in WT tissue than Q175 tissue, possibly implicating this as the source of higher Kyn in WT brain.

3.3. Effects of oral administration of Kynurenine to mice

It is conceivable that the changes in CNS Kyn catabolism following KMO block may have resulted purely as a consequence of sensing grossly elevated Kyn levels. As Kyn can be dosed orally to produce increases in plasma and CNS Kyn levels, we tested the profile of CNS KP metabolite generation on Kyn bolus administration when KMO is not inhibited. Prior experiments had determined that the Kyn levels in plasma are similar after a 30 mg/kg oral dose of either Kyn or CHDI-340246, and this was determined here as well (Fig. 3). In this study, we monitored the levels of KP metabolites in the striatal extracellular space over a 4 h period in response to either 30 mg/kg Kyn or 30 mg/kg CHDI-340246 bolus administration, and obtained measurements at 2 time points, at $t = 1$ h and 5 h post dosing, from cortex, striatum, kidney, and liver as well as plasma (Fig. 3; Figs. S3 and S4).

The administration of an oral dose of Kyn lead to elevations in Kyn to the same extent as that seen with CHDI-340246 (Fig. 3A). However, the profile of subsequent Kyn catabolism was significantly shifted towards the generation of predominantly 3-OH-Kyn and KynA (Fig. 3B, D). Levels of KynA were increased 26-fold after a 30 mg/kg dose of Kyn, whereas after a 30 mg/kg po dose of CHDI-340246, KynA extracellular levels increased by 63-fold (Fig. 3B). Levels of 3-OH-Kyn were increased 23-fold after Kyn administration versus 3.4-fold after CHDI-340246 dosing (Fig. 3D). In contrast and suggestive of a differential metabolism in mice, AA levels were less affected by exogenous Kyn dosing (Fig. 3C). These results suggest that in response to a systemic flux of Kyn, its catabolism is the brain is mediated mostly by KMO and KATs, but not kynureninase. The elevations in 3-OH-Kyn and Quin were also very significant in all tissue homogenates measured (striatum, cortex, kidney and liver; Figs. S4 and S5), although the elevation in KynA and AA in liver and kidney are much more muted. This finding confirms KMO block by CHDI-340246 alters CNS Kyn catabolites in a way distinct from Kyn administration, and underscores that Kyn administration

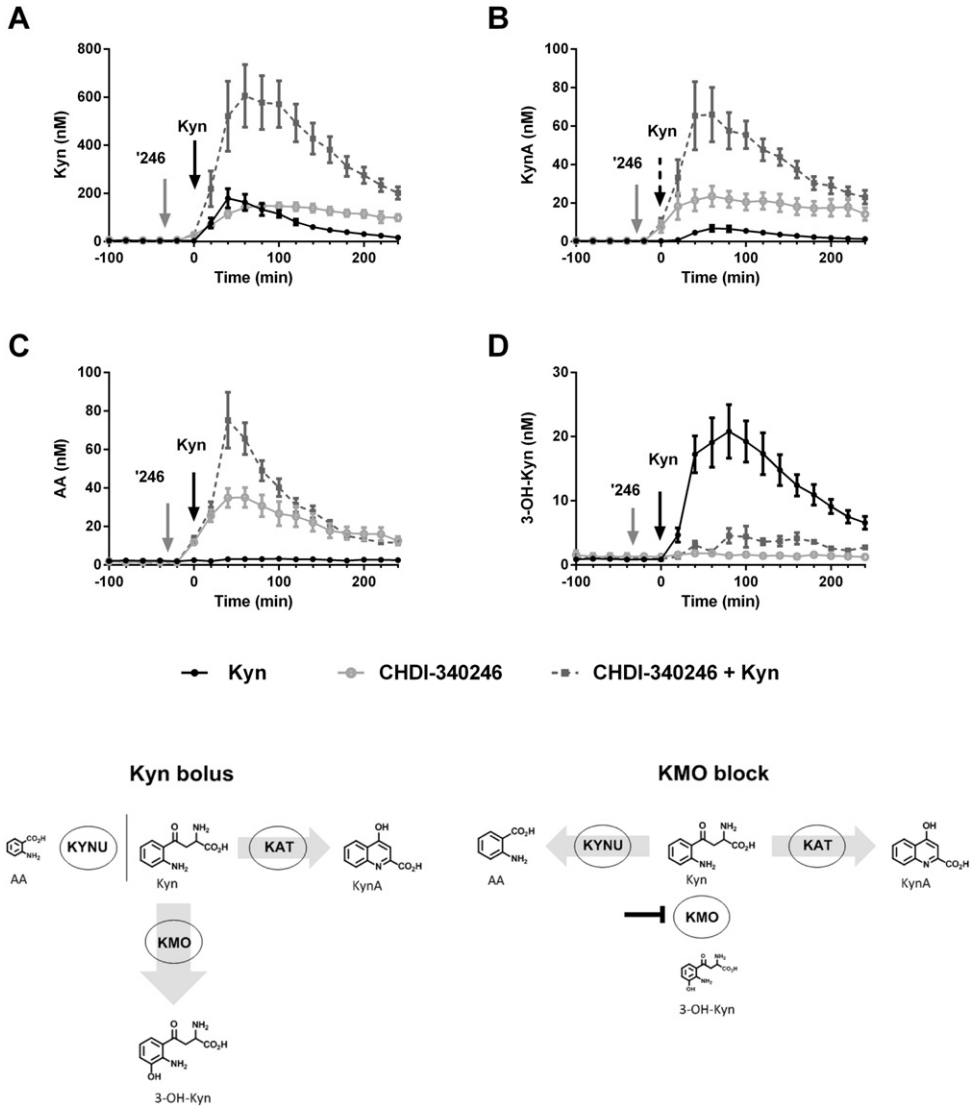

Fig. 3. Pharmacodynamic effects of oral co-administration of CHDI-340246 and kynurenine in wildtype mice. CHDI-340246 (30 mg/kg po) is administered to wildtype mice at $t = -30'$ (grey arrow) either alone (grey open circles) or in combination with Kyn (grey closed squares). At $t = 0$, 30 mg/kg po Kyn is administered (black arrow) either alone (black closed circles) or following dosing of CHDI-340246 (grey closed squares). Microdialysis probes are implanted in the striatum and samples are collected in 20 min intervals. Levels of various kynurenine metabolites are shown (A-D). Cartoons exemplify the major route of Kyn catabolism following Kyn bolus administration, versus KMO inhibition following CHDI-340246 administration.

will not produce the same effects as CHDI-340246 in terms of the desired CNS KP metabolite profile.

3.4. Oral co-administration of 30 mg/kg CHDI-340246 with 30 mg/kg Kynurenine suggests KMO inhibition in brain tissues

Finally, in order to demonstrate CNS inhibition of KMO activity following systemic CHDI-340246 dosing, we pre-dosed Kyn orally ($t = -30$ min, 30 mg/kg) followed by an oral administration of CHDI-340246 at 30 mg/kg ($t = 0$ min; Fig. 3A). When co-administered, CHDI-340246 reduced the elevation of brain extracellular levels of 3-OH-Kyn and Quin induced by Kyn dosing by 75–90% (Fig. 3) and 60–80% (data not shown), respectively (Fig. 3D and not shown). In cortex homogenates, the levels of 3-OH-Kyn and Quin are decreased by 88% and 69%, respectively at $t = 1$ h after Kyn is co-administered with CHDI-340246 (Fig. S5). Similar findings occur in other tissues (Figs. S4 and S5). Quin levels in brain tissue can partially originate from the blood compartment (Fukui et al., 1991; Heyes and Morrison, 1997). The profound inhibition of 3-OH-Kyn centrally is likely a consequence of CNS blockade of KMO at this dose, although definitive proof would require a metabolic labeling study to ascertain the extent of inhibition of *de novo* synthesis of 3-OH-Kyn in the brain (Amori et al., 2009).

The increased generation of KynA and AA in the studies with CHDI-340246 and in the co-dosing paradigm supports that there is a CNS block of KMO activity at this dose (Fig. 3A-C). Given the influx of several metabolites into the brain from the periphery via circulating blood (Fukui et al., 1991; Heyes and Morrison, 1997; Kita et al., 2002), the greater than additive response to combined dosing of Kyn and CHDI-340246 (particularly the effect on AA; Fig. 3C) is indicative that AA is primarily produced from Kyn in the CNS when KMO is blocked in the brain through the local production of Kyn. This is consistent with results obtained from the study of KMO knockout mice (Giorgini et al., 2013).

3.5. Neither KMO inhibition by CHDI-340246, nor direct application of KP metabolites, impact basal glutamatergic transmission, but rescue hippocampal LTP deficits in R6/2 mice

PD evaluation of the CNS KP metabolites following systemic CHDI-340246 administration demonstrated that Kyn, KynA, and AA are elevated in response to the compound. Importantly, these quantitative microdialysis studies for the first time provided reliable concentration estimates of the metabolites present in the interstitial fluid following dosing. For dose levels of CHDI-340246 between 10 and 100 mg/kg po in Q175 hets, brain Cmax achieved was between 75 and 280 nM for Kyn, and between 15 and 30 nM for both KynA, and AA. In contrast, maximum concentration achieved for 3-OH-Kyn was only 1.6–2 nM from a baseline mean level of 0.8 nM. At 10 mg/kg po, CNS CHDI-340246 C_{max} from total brain homogenate was determined to be 0.8 ± 0.06 μM. We thus used these values as guideline concentrations to investigate the potential beneficial effects of KMO inhibition in HD models, firstly using *ex vivo* investigation of metabolite and compound action in both hippocampal and cortico-striatal acute brain slices from R6/2 and Q175 mice.

Fig. 4 shows the evaluation of direct CHDI-340246 and KP metabolite administration on glutamatergic synaptic transmission in corticostriatal and hippocampal slices prepared from 8 week old symptomatic R6/2 mice and WT littermates. We have previously shown that at this age, evoked corticostriatal excitatory postsynaptic currents are impaired in R6/2 mice (Mielcarek et al., 2013), as indicated by a rightward shift in the I-O (I—O) response of EPSCs measured in SPNs following cortical Layer V stimulation (2 Way ANOVA; $p < 0.0001$). Application of 1 μM CHDI-340246 to slices for 30–50 min had no effect on the I—O curves in either WT or R6/2 slices (Fig. 4A).

In a higher throughput system, we also evaluated CHDI-340246 (1 μM) or the KP metabolites; Kyn (50 nM), KynA (100 nM), AA (100 nM) and Quin (1 μM), on CA3:CA1 synaptic transmission in hippocampal slices from R6/2 and WT mice. CHDI-340246 did not affect CA3:CA1 transmission, assessed either by stimulus-response size in WT or R6/2 mice (Fig. 4B), or by paired pulse ratio analysis (Fig. 4C; R6/2 data shown); WT PPR was also unaffected in response to drug ($n = 13$, $p = 0.4$, data not shown). Neither KynA (100 nM), AA (100 nM) or Quin (1 μM, applied vastly in excess to physiological basal levels in HD models; Fig. 4D–F) affected basal synaptic transmission. Kyn application produced a very modest but significant inhibition of transmission (≤5% reduction of fEPSP amplitude; Fig. 4G). We conclude that there is no effect of KMO inhibition or the KP metabolites KynA or AA on fast glutamatergic transmission in either striatum or hippocampus, as measured *ex vivo*, while Kyn showed a very small inhibition of transmission.

We additionally measured striatal extracellular glutamate levels by microdialysis in response to acute systemic CHDI-340246 administration (10 and 100 mg/kg po in Q175 (Fig. 4G) and WT mice (Fig. 4H). CHDI-340246 failed to modulate baseline levels. This latter data contradicts previous reports conducted in rats, which showed that the KMO inhibitor Ro 61–8048 (40 mg/kg ip) (Rover et al., 1997), or reverse dialysis of 100 nM KynA (Moroni et al., 2005), could decrease extracellular glutamate levels in caudate, which was later ascribed to block of presynaptic α7 nicotinic acetylcholine receptors (α7 nAChRs) (Konradsson-Geuken et al., 2010). We therefore performed further *in vitro* experiments to characterize the pharmacological profile of KP metabolites at α7 receptors. In our hands, Kyn and KynA effects at α7 nAChRs were negligible in the sub μM range, and we found no evidence to suggest that they could act as nicotinic α7 receptor antagonists (Fig. S6 and Table S5).

Next, we examined the effects of CHDI-340246 and KP metabolites on excitatory synaptic plasticity in the hippocampus. Symptomatic R6/2 mice exhibit a deficit in classical NMDA-dependent LTP at hippocampal CA3-CA1 synapses (Beaumont et al., 2014; Murphy et al., 2000). Using multi-electrode array (MEA) field recordings, we confirmed that theta-burst stimulation (TBS) induces significantly less potentiation in R6/2 compared to WT (Fig. 5). Surprisingly, this deficit was fully rescued by acute application of CHDI-340246 (1 μM; Fig. 5A), and to a lesser but significant extent by two structurally unrelated KMO inhibitors; UPF-648 (Amaral et al., 2013) (10μM) and Ro-61-8048 (Rover et al., 1997)(data not shown). These inhibitors presumably work by acutely elevating either AA, Kyn or KynA in the slice. Direct application of Kyn (50 nM) mimicked the rescue seen with CHDI-340246 ($p < 0.01$), Fig. 5B). 100 nM KynA showed a non-significant trend towards improvement ($p = 0.07$; Fig. 5C), whilst AA (100 nM) was completely ineffective (Fig. 5D). These results suggest that the effects of KMO inhibition on restoring hippocampal LTP deficits are driven primarily by the elevation of Kyn (and possibly to a lesser extent KynA); and not via driving Kyn catabolism towards AA production, nor via reduction in 3-OH-Kyn or Quin levels. We tested whether Quin (1 μM) resulted in further deficits in R6/2 LTP, but we found no effect (Fig. 5E). It should be noted that this concentration is vastly higher than either the basal Quin level in HD mice (~4 nM) or the level achieved following CHDI-340246 dosing (6 nM). Of the compounds that improved R6/2 LTP deficits, notably neither CHDI-340246, Kyn nor KynA had any significant effect on LTP in WT hippocampal slices. We conclude that CHDI-340246 and Kyn are capable of a selective restoration of deficient synaptic plasticity in R6/2 hippocampal CA3-CA1 synapses.

It is worth mentioning that as the process of LTP explicitly requires NMDA receptor activation, rescue of LTP deficits would be inconsistent with an alleged antagonism of NMDA receptors. Given that the IC_{50} for NMDA receptor inhibition by KynA is reported to be much higher than the free concentrations we measured following physiological KMO block, or applied here, this is perhaps not surprising (Mok et al., 2009). Our measurements confirmed the low potency for KynA at NMDA receptors in a heterologous cell system; IC_{50} was 26 ± 11 μM at NR2A containing receptors, and 499 ± 54 μM at NR2B containing receptors (Fig. S7). Other KP metabolites were also tested for both agonist and antagonist effects on NMDA receptors. This data confirmed that even at 300 μM Quin, activation or potentiation of submaximal NMDA currents was negligible, and other KP metabolites were without effect

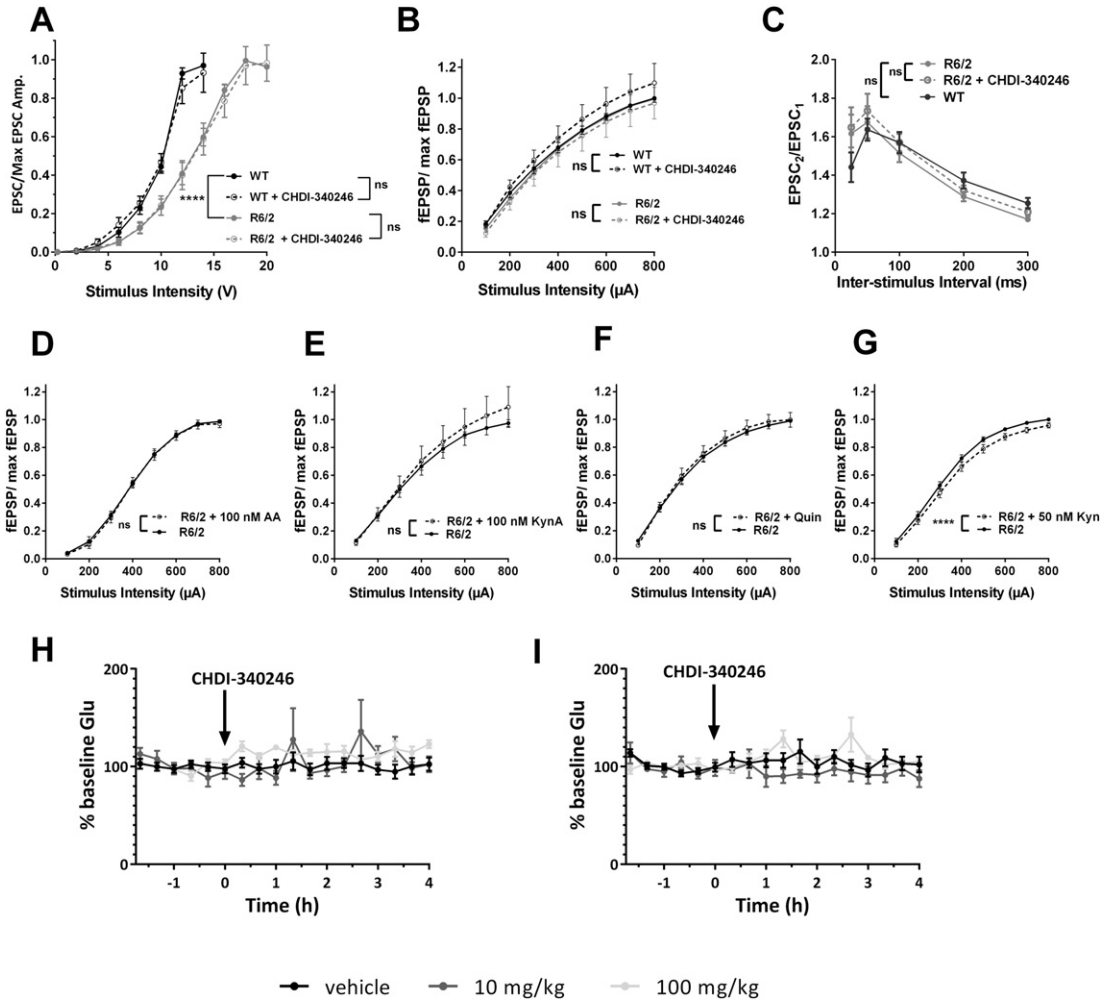

Fig. 4. Acute KMO inhibition does not result in modulation of glutamatergic transmission. (A) EPSC I—O curves in R6/2 corticostriatal slices in response to Layer V stimulation are right-shifted compared to WT littermates, indicating reduced responsiveness of R6/2 SPNs to cortical stimulation. A subsequent application of CHDI-340246 (1 μM), applied for 30–50 min to either R6/2 or WT corticostriatal slices, had no effect on SPN EPSC amplitudes at either submaximal or maximal stimulus intensities ($n = 10$ slices per group). (B–C) CHDI-340246 was equally ineffective in modulating glutamatergic transmission at either R6/2 or WT hippocampal CA3: CA1 synapses, measured both by lack of effect on I—O curves (B) or on paired pulse ratios (C, WT, R6/2 and R6/2 following compound shown), $n = 11$–12 slices per group. (D–G) Acute application of 100 nM AA (D), 100 nM KynA (E) or 1 μM Quin (F) did not modulate glutamatergic transmission at hippocampal CA3: CA1 synapses, however 50 nM Kyn (G) produced a very modest decrease in transmission (D–G: 9–11 slices per condition tested). (H—I). Systemic dosing of CHDI-340246 (10 or 100 mg/kg po) to either Q175 hets (H) or WT (I) mice did not modulate striatal interstitial glutamate levels, monitored through microdialysis probes. Veh = vehicle control. Repeat measures 2-way ANOVA *ns* = non-significant, $^{****}p < 0.0001$.

measured up to 100 μM (Fig. S7). We further explored whether the main KP metabolites had any direct activity on a variety of receptors, including Kainate, AMPA, and $GABA_A$. None exhibited significant binding against these targets (Table S5). Taken together, these results suggest that the effects of CHDI-340246, Kyn and KynA in our assays likely do not involve a direct modulation of major ionotropic receptors in the brain as had been previously proposed.

3.6. CHDI-340246, Kyn and KynA acutely restores R6/2 SPN membrane excitability

We next assessed the effects of KMO block, Kyn and KynA on intrinsic membrane properties of striatal SPNs, a cell type which is extremely vulnerable to mHtt insult. R6/2 and Q175 SPNs are aberrantly hyperexcitable relative to their WT counterparts, characterized by modest resting membrane potential depolarization (Fig. 6A), increased membrane resistance (Fig. 6B) and decreased rheobase (Fig. 6C). At 5–7 weeks in R6/2 (earlier than the age studied here), D2 receptor expressing SPNs (putative indirect pathway SPNs) are reported to be preferentially affected (Cepeda and Levine, personal communication from data generated from Cepeda et al., 2013), while at 6 months of age in Q175, both D1 and D2 receptor expressing SPNs are similarly affected (CHDI; unpublished data). We found that a direct application of CHDI-340246 acutely hyperpolarized SPNs ($p < 0.05$; Fig. 6A) and decreased Rm ($p < 0.0001$; Fig. 6B) in R6/2 SPNs. Analysis of drug action on each neuron showed that all neurons hyperpolarized in response to CHDI-340246, suggesting that this effect was common to both D1 (direct pathway) and D2 (indirect pathway) SPNs (data not shown). WT SPNs were also somewhat responsive to the drug, although the hyperpolarization (ns, $p = 0.18$) and changes in Rm ($p < 0.05$) were more muted than seen in the depolarized HD neurons. CHDI-340246 also affected rheobase; in this case, WT neurons showed significantly increased rheobase ($p < 0.001$), while R6/2 neurons showed a non-significant trend towards restored rheobase ($p = 0.1$). Acute application of KynA (100 nM) or Kyn (50 nM) replicated the effects of CHDI-0340246, hyperpolarizing R6/2 SPNs (Fig. 6D). The effect of CHDI-340246 and Kyn was rapid, inducing an outward (hyperpolarizing) current within approximately 5 min of application (Fig. 6E). The effect of KynA application appeared more biphasic, with a modest transient depolarization preceding hyperpolarization.

Hyperpolarization, decreased input resistance, and increased rheobase are all consistent with a CHDI-340246-induced increase in

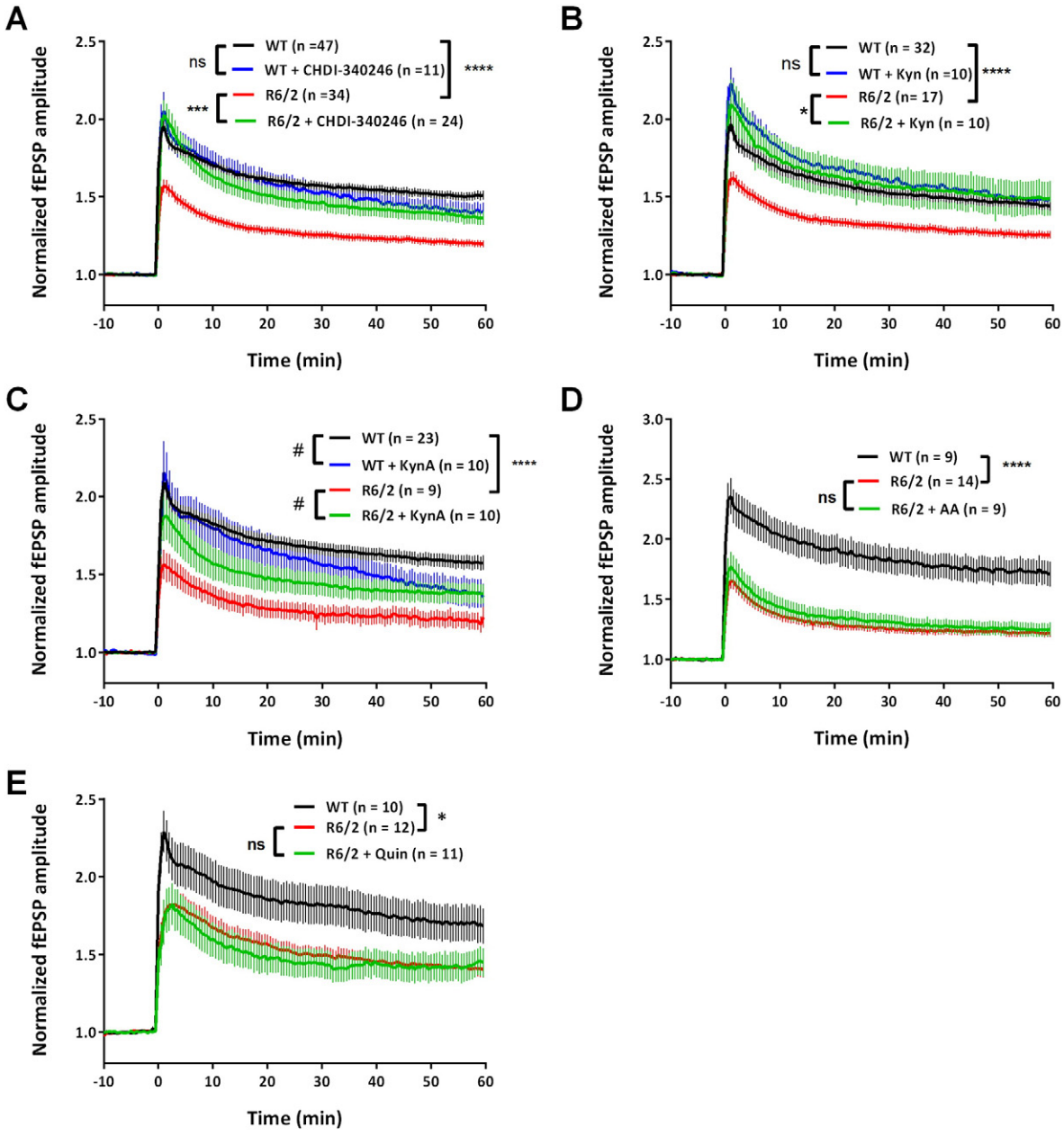

Fig. 5. Acute inhibition of KMO or application of Kyn reversed R6/2 hippocampal LTP deficits. Data are expressed as mean ± sem fEPSP amplitude normalized to a 10 min baseline period prior to induction of LTP by theta-burst stimulation at $t = 0$ min. Acute application of CHDI-340246 (1 μM; A) or Kyn (50 nM; B) to hippocampal slices prepared from 8 week old mice resulted in selective rescue of R6/2 LTP deficits. KynA (100 nM; C) showed a modest non-significant trend for rescue of R6/2 LTP ($p = 0.07$), while AA (100 nM; D) or Quin (1 μM; E) was without effect. CHDI-340246, Kyn and KynA had no effect on WT LTP amplitude (A–C). Repeat measures 2-way ANOVA at time t = 20–60 min: #, $p < 0.1$,*$p < 0.05$, ***$p < 0.001$, ****$p < 0.0001$. n = number of slices recorded.

potassium conductance, key ion channels which underlie pathological alterations in HD cells (Ariano et al., 2005; Cepeda et al., 2003; Tong et al., 2014; Waters et al., 2013). Indeed, clamping R6/2 SPNs at Vh further from putative E_K (−90 mV) exacerbated the effects of CHDI-340246 on changes in Rm (Fig. 7A), while clamping the cells at −95 mV, close to E_K, abrogated the effect, supporting modulation of an underlying potassium conductance as responsible for the improvement.

Of interest, in separate studies, we have shown that Rm abnormalities in HD models can also be acutely rescued in R6/2 and Q175 SPNs by the phosphodiesterase inhibitors PDE10, PDE2 and PDE9; which elevate cyclic nucleotide (cAMP and/or cGMP) levels. These PDE inhibitors are also capable of reversing R6/2 hippocampal LTP impairments (see http://chdifoundation.org/2012-conference-2/#beaumont). In line with this, Fig. 7B and Fig. 7D show that 15 min application of a cell permeable analog of cGMP, 8-Br-cGMP (1 μM), produces effects indistinguishable to CHDI-340246 on Rm and Im effects, an effect which shows partial inhibition following pre-incubation of slices with the PKG inhibitor KT5823 (0.5 μM; Fig. 7B). As there is precedence that Kyn can act as a modulator of nitric oxide signaling in vascular endothelium producing cGMP (Wang et al., 2010), this raised the interesting possibility that central KMO inhibition may also enhance cGMP levels to produce the beneficial effects in SPNs. We tested this by determining whether CHDI-340246 effects on R6/2 SPN excitability changes were sensitive to combined adenylyl cyclase and guanylyl cyclase block by pre-incubation of slices with SQ 22536 (10 μM) and ODQ (10 μM), or mitigated by KT5823-induced PKG inhibition (0.5 μM). Fig. 7C and D shows that this at least partially the case; with significant inhibition of Rm changes (Fig. 7C) and an almost full inhibition of the generation of the outward membrane current induced by CHDI-340246 application (Fig. 7D).

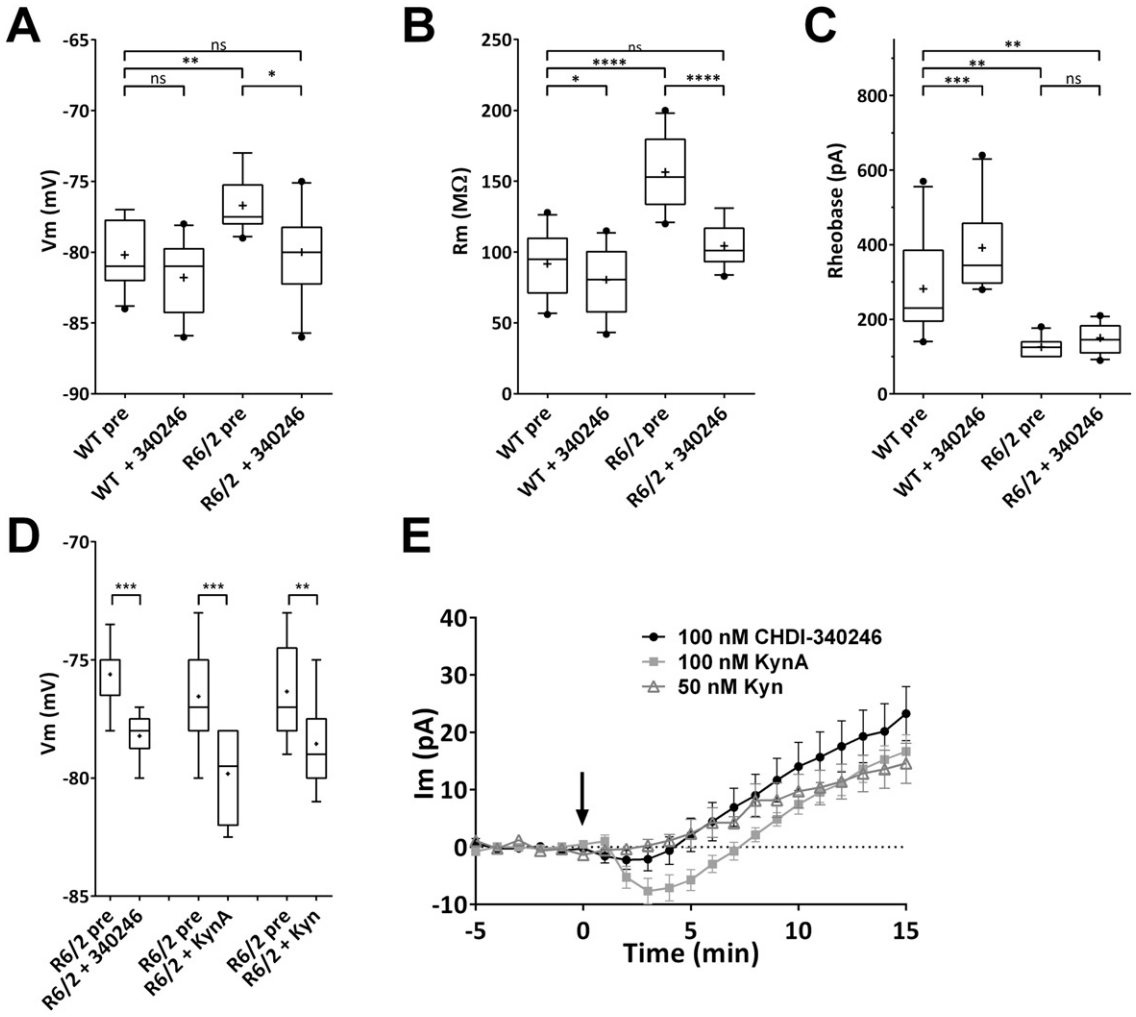

Fig. 6. CHDI-340246, Kyn and KynA acutely restored R6/2 SPN membrane excitability. (A-C) CHDI-340246 (100 nM) effects on resting membrane potential Vm (A), membrane resistance Rm (B) and rheobase (C) in WT and R6/2 SPNs. R6/2 SPNs are characterized by modest depolarization (A), increased Rm (B) and decreased rheobase (C) compared to WT SPNs, indicating aberrant excitability. CHDI-340246 acutely hyperpolarized R6/2 SPNs (A) and decreased Rm (B); while this latter effect was also noted in WT SPNs, the effect on Rm is more profound in R6/2 SPNs. (C) CHDI-340246 increased rheobase in WT SPNs, but did not significantly affect R6/2 SPNs. (D) Acute application of KynA (100 nM) or Kyn (50 nM) are as effective as CHDI-340246 in hyperpolarizing R6/2 SPNs. Data are presented as box (25–75th percentile) and whisker (10–90th percentile) plots. Line indicates median and + indicates mean value. Outliers are indicated by closed symbols. (E) Time-course of acute CHDI-304246, Kyn or KynA application on baseline adjusted SPN membrane current. Mean ± SEM shown. Kyn and CHDI-340246 induce an outward (hyperpolarizing current) within minutes of application, whereas the effect of KynA appears more biphasic, with a modest transient depolarization preceding hyperpolarization. $^{*}p < 0.05$, $^{**}p < 0.01$, $^{***}p < 0.001$, $^{****}p < 0.0001$. ($n = 9$–11 neurons per condition for all panels).

Together, this data provides evidence that Kyn [and KynA] elevations following KMO inhibition are likely responsible for a potassium conductance-mediated hyperpolarization of HD SPNs towards WT levels, in a way which appears to implicate a role for CHDI-340246 and Kyn in modulating cyclic nucleotide signaling pathways.

3.7. In vivo efficacy studies evaluating the effects of chronic inhibition of KMO in mouse models of HD

Given the dose-dependent effects on modulating peripheral and CNS levels of KP metabolites by CHDI-340246, we assessed whether it could ameliorate electrophysiologically assessed disease phenotypes in HD models following chronic administration. We dosed two HD mouse models (R6/2 and Q175 hets) with either vehicle or 10–30 mg/kg CHDI-340246 po bid, from a presymptomatic age (4 weeks of age in R6/2, or 2 months of age in Q175) to an age where the mice without drug are symptomatic. Thus, in R6/2 mice, readouts were conducted at 8 or 12 weeks of age (following 4–8 weeks of dosing at 10 and 30 mg/kg), and in Q175 hets at 6 months (following 4 months of dosing, 10 mg/kg only). Slices were prepared from treated mice either 3 days (R6/2) or between 3 and 14 days (Q175) post last dose. Using this format, any restoration of neuronal or synaptic function seen as a result of treatment would result from a beneficial effect of the dosing strategy on delaying or preventing HD pathophysiology (ie disease modification), and could be distinguished from any acute actions of the drug.

As previously described, the major genotypic differences between HD and WT SPNs are an increase in membrane resistance and decreased rheobase, as well as impaired glutamatergic transmission. The CHDI-340246 dosing paradigm failed to show any preventative restoration of elevated SPN Rm, rheobase (Fig. 8A) or Vm (data not shown) in either R6/2 or Q175 mice, suggesting that the drug must be actually present to exert its effect on these phenotypes (i.e. an acute symptomatic action). To assess any potential improvement in impaired striatal glutamatergic transmission, in this study miniature EPSCs were recorded. mEPSC frequency but not amplitude is significantly decreased in both R6/2 and Q175 het SPNs, as compared to those from aged matched WT mice, indicating either a paucity of striatal glutamatergic innervation or reduced probability of glutamate release (Fig. 8B–C) which may arise from both cortical and/or thalamic origin. In Q175 mice following 4 month dosing, these mEPSC frequency deficits were completely prevented by CHDI-340246 (Fig. 8B; $p < 0.001$). There was no effect of 10 mg/kg CHDI-340246 on mEPSC amplitude or frequency in the corresponding WT

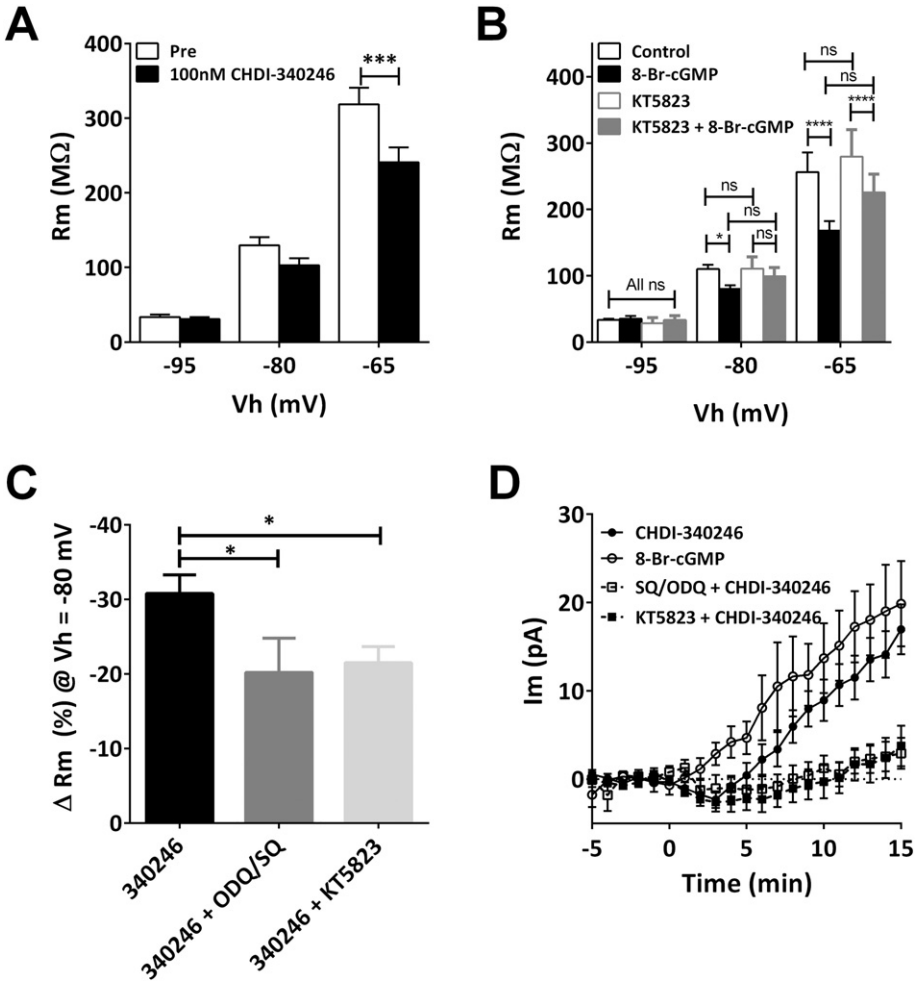

Fig. 7. CHDI-340246 modulation of potassium conductance via cyclic nucleotide modulation likely accounts for changes in SPN excitability. A. Change in 8 week old R6/2 SPNs Rm following acute CHDI-340246 application is abrogated when Vh is clamped at −95 mV close to E_k, and exacerbated when Vh is held at more depolarized potentials, suggesting the modulation of a potassium conductance underlies the effect ($n = 8$). B. Change in R6/2 SPN Rm seen with CHDI-340246 is mimicked by acute application of 1 μM 8-Br-cGMP ($n = 5$). Pre-incubation with the PKG inhibitor KT5823 modestly diminished the cGMP response ($n = 8$). **C.** Change in Rm in R6/2 SPNs by CHDI-340246 ($n = 10$) is partially inhibited by preincubation with the AC and GC inhibitors SQ 22536 (SQ) and ODQ (both 10 μM; $n = 8$), or by preincubation with KT5823 ($n = 11$), suggestive that elevation of cyclic nucleotide levels by KMO inhibition partially underlies the response. D. Changes in R6/2 SPN Im with CHDI-340246 ($n = 19$), responsible for hyperpolarization of SPNs, is mimicked by 8-Br-cGMP ($n = 8$), and significantly attenuated following preincubation with SQ/ODQ ($n = 8$) or KT5823 ($n = 11$). Statistics by one or two way ANOVA with Sidak's multiple comparison test as appropriate; * $p < 0.05$; *** $p < 0.001$; **** $p < 0.0001$.

littermates dosed for a similar period of time. In the more severe and rapidly progressing R6/2 mouse model, a 30 mg/kg (but not 10 mg/kg) CHDI-340246 dosing regimen resulted in a partial, significant improvement in mEPSC frequency (Fig. 8C; $p < 0.05$). Given the previous WT findings in Q175 mice, CHDI-340246 dosed WT groups were omitted from this study.

The more significant effect of the long-term dosing regimen in Q175 hets might be explained by a more protracted disease course, or the longer period of treatment, but in both models we demonstrated that CHDI-340246 can partially ameliorate some neurophysiological readouts associated with disease. In combination with our findings using an acute dosing regime, our combined results demonstrate that KMO inhibition results in 1) acute effects on HD SPNs resulting in hyperpolarization and restoration of aberrant membrane properties, driven by nM levels of Kyn and KynA elevation; 2) specific restoration of deficient synaptic plasticity in hippocampal CA3:CA1 synapses driven mainly through nM levels of Kyn elevation, and 3) an improvement in functional glutamatergic input to the striatum brought about by a long-term application. In contrast to prior reports by others, we do not find evidence that any of these actions are being mediated through either NMDA receptor blockade, or through nicotinic alpha 7 receptor blockade. In fact, our results suggest that the acute improvement in HD related phenotypes described here are mediated, at least to a large part, by the nM elevation of kynurenine afforded by KMO block.

3.8. Behavioral evaluation of R6/2 mice treated with CHDI-340246

We conducted an extensive set of studies aimed at evaluating the chronic effects of KMO inhibition on comprehensive measures of disease in HD models, using behavioral, molecular, lifespan and brain volumetric readouts (Figs. 9 and 10; Fig. S8 and Table S3). For behavioral studies, we focused our studies on Q175 homs and R6/2 mice. Q175 hets do not display significant and robust locomotor deficits before 8 months of age (Heikkinen et al., 2012; Menalled et al., 2012), so we chose Q175 homs for behavioral endpoints. CHDI-340246 was tested in R6/2s at 10, 30 and 100 mg/kg (to ensure coverage of peripheral and CNS KMO activity) from 4 to 12 weeks of age po bid, and from 5 weeks to 9 months of age in Q175 homs at 0.1, 1 and 10 mg/kg po bid (the low doses were chosen to match the small elevations in Kyn and KynA levels as reported (Zwilling et al., 2011).

Motor function endpoints including open field and rearing/climbing tests were conducted for the R6/2 study at 4 weeks of age (baseline) and at 6, 8, 10 and 12 weeks ($n = 19$–20 R6/2 mice/dose, and n = 20 WT mice (equal gender split). Accelerated rotarod testing was performed

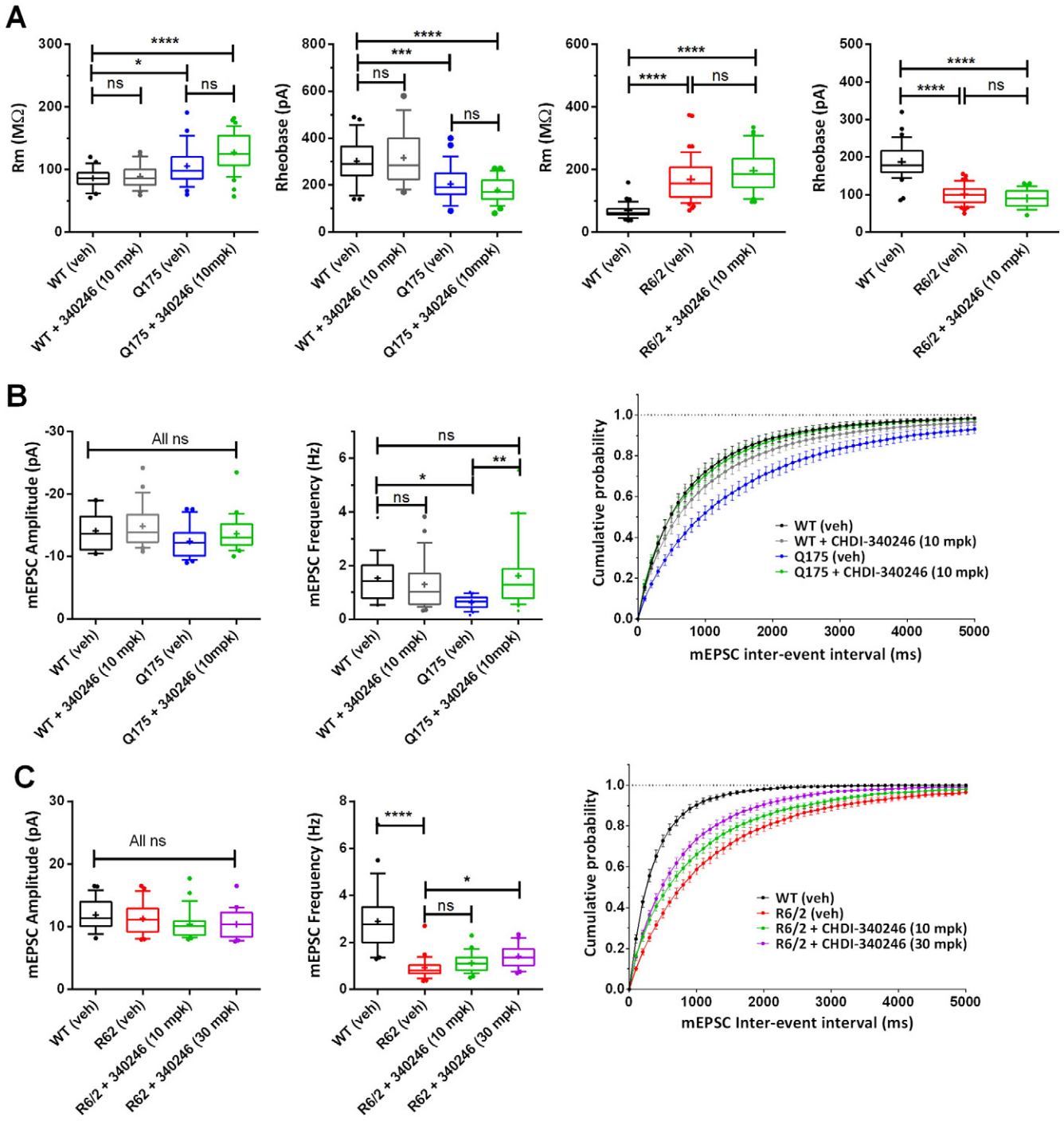

Fig. 8. Chronic dosing of CHDI-340246 in R6/2 and Q175 mice results in rescue of mEPSC frequency deficits in striatum. (A–C). Q175 het or R6/2 mice were treated chronically (10–30 mg/kg po bid) with vehicle or CHDI-340246 for 4 or 8 weeks (R6/2, from 4 to 8 or 4–12 weeks) or 4 months (Q175, from 2 to 6 months) alongside vehicle treated WT littermates. *Ex vivo* evaluation of improvement in neurophysiological measures were made from acute slices 3 d (R6/2) or 3–14 d (Q175) post-last dose. (A) Aberrant excitability in Q175 or R6/2 SPNs, as measured by elevated Rm and decreased rheobase, were not rescued by the chronic dosing paradigm employed (R6/2 dosed from 4 to 8 weeks) $n = 22–44$ neurons per group. (B–C) The decrease in average mEPSC frequency in HD models (B; Q175, C; R6/2), with no change in mEPSC amplitude, reflects impaired glutamatergic release in striatum, indicated by a right-shifted inter-event interval cumulative probability curve in the HD models. **(B)** Chronic dosing with 10 mg/kg CHDI-340246 in Q175 mice fully prevented this phenotype from emerging. $N = 17–26$ neurons per group **(C)** In R6/2 mice dosed for a shorter time period of 8 weeks (from 4 to 12 weeks of age), 30 mg/kg but not 10 mg/kg resulted in significant partial restoration of mEPSC frequency deficits. $N = 20–28$ neurons per group.

at 4, 6, 8 and 10 weeks. Grip strength test was performed at weeks 4, 10 and 12. For the Q175 hom study, $n = 19–20$ female and male Q175 hom mice/dose and n = 19 WT littermate control mice were used. Body weight was measured weekly starting at the age of 5 weeks and continued until the end of the study. Neurological index was performed at 4 and 8 months of age. The open field and rear climbing tests were conducted at 5 weeks of age (baseline) and at 4 and 8 months. A description of all studies conducted is shown in Table S3. CHDI-340246 was very well tolerated in both HD models, with no change in body weight (Fig. 9A and Fig. S8), neurological scores or sedation (not shown), even at the high dose of 100 mg/kg.

In the R6/2 study, we failed to observe any consistent locomotor effects of the drug, as judged by the open field (distance traveled, average velocity) or rearing tests or the accelerated rotarod test (Fig. 9C–D

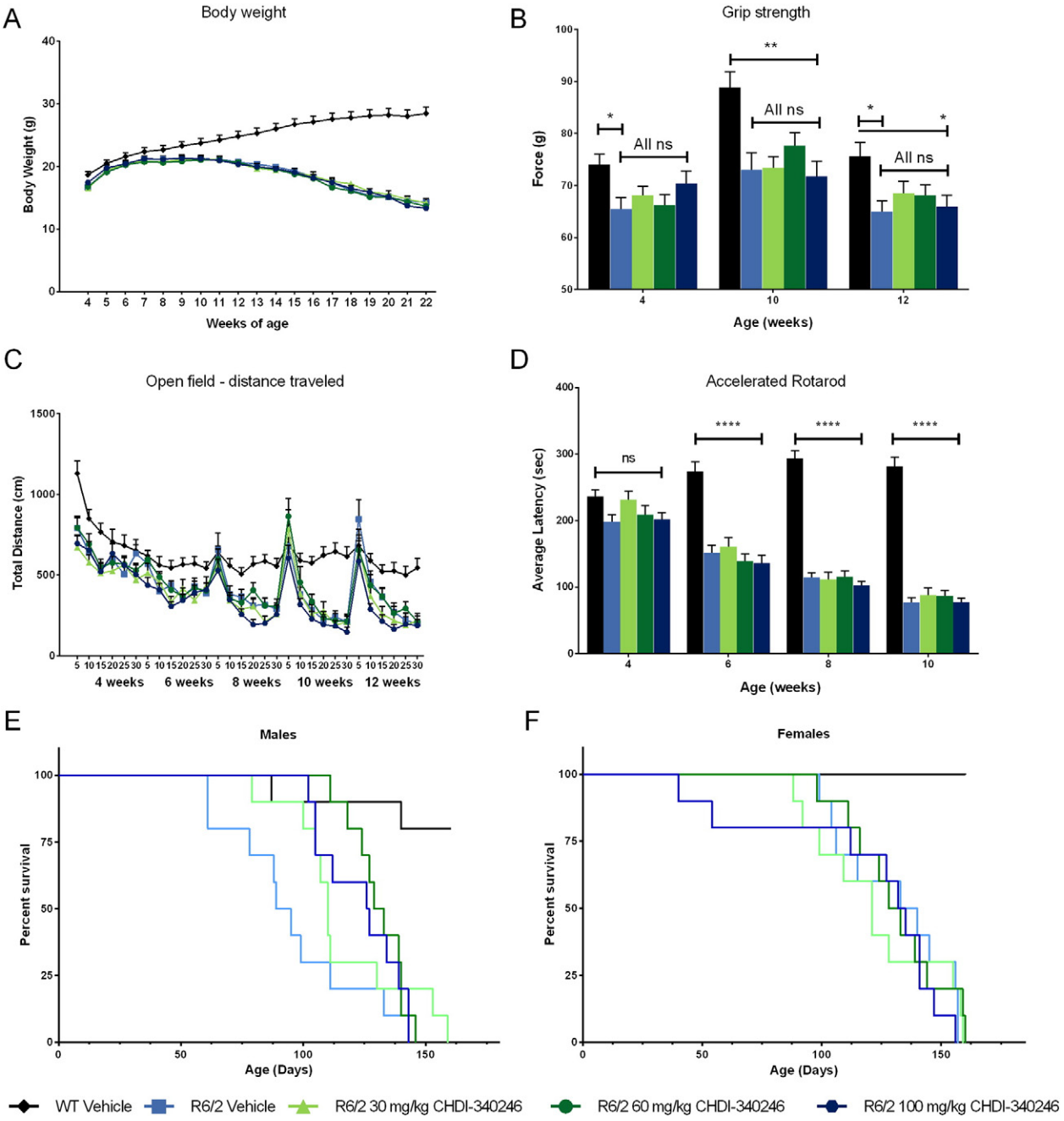

Fig. 9. Effects of CHDI-340246 chronic administration in WT and R6/2 mice. Animals were chronically dosed (po bid) with CHDI-340246 from 4 weeks of age at either 30, 60 or 100 mg/kg. There were no observable effects in (**A**) body weight, (B) grip strength, (C–D) locomotor activity, as reported here using the open field distance traveled (C), and the accelerated rotarod (D). Body weight, open field, grip strength and rotarod performance between WT and R6/2 mice were highly significant (*, $p < 0.05$; **, $p < 0.01$; ****, $p < 0.0001$; ns = not significant; One Way ANOVA, Tukey's post-hoc multiple comparison test). (**E, F**) Within males only, mice treated with 60 and 100 mg/kg of CHDI-340246 had improved median survival rates compared to vehicle treated R6/2 mice ($p < 0.05$; Generalized Wilcoxon, Peto-Prentice).

shows data pooled for all animals; other parameters not shown). At the 100 mg/kg dose, R6/2 female mice traveled less distance during the task at weeks 8–12 (not shown). Grip strength measurements revealed a beneficial effect of the drug in female mice only at 60 mg/kg at 10 weeks (not shown), but we could not detect any improvement in male mice (Fig. 9B shows grip strength results using data from pooled animals, with no effect of CHDI-340246). Similar lack of effects on motor endpoints was observed in Q175 homs (Fig. S8).

In R6/2 mice, we also monitored lifespan (n = 20 animals/group). The mean/median survival times of the R6/2 mice treated with vehicle were 114/106 days for pooled genders, 131/140 days for females and 96/95 days for males. The mean/median survival times of the R6/2 mice treated with 30 mg/kg of CHDI-340246 were 110/120 days for pooled genders, 123/121 days for females and 116/110 days for males. For the 60 mg/kg dose, survival times were 131/129 days for pooled genders, 131/133 days for females and 131/133 days for males. For the 100 mg/kg group, survival times were 121/127 days for pooled genders, 119/135 days for females and 124/127 days for males. Within males both the mice treated with 60 and 100 mg/kg of CHDI-340246 had improved survival rates compared to vehicle treated R6/2 mice (Generalized Wilcoxon, Peto-Prentice: $p < 0.05$; Fig. 9E–F).

Finally, we monitored for potential effects of CHDI-340246 on brain volumetric loss and other measures associated with neurodegeneration

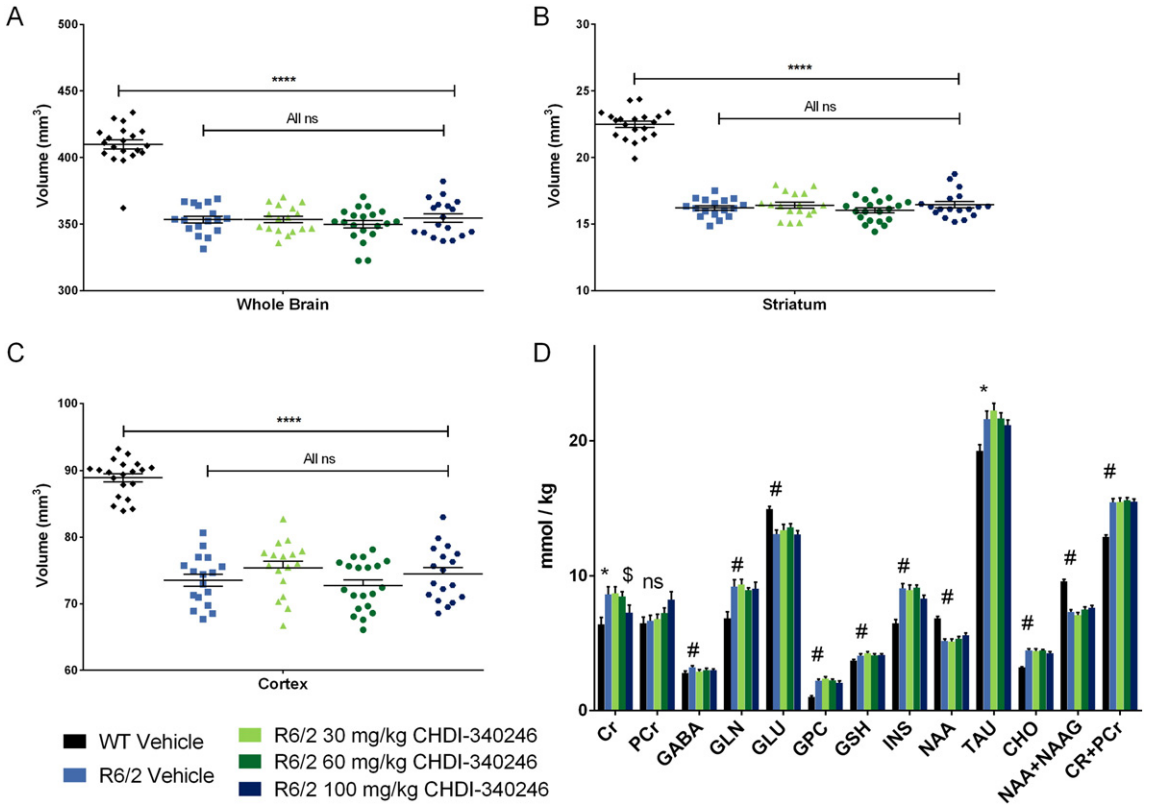

Fig. 10. Effects of CHDI-340246 chronic administration on brain volumetric alterations and MRS in R6/2 mice at 12 weeks of age. The effect of chronic administration of CHDI-340246 on whole brain volumes as shown by MRI of the pooled genders of R6/2 mice at 12 weeks of age. Data are presented as scatter plots with mean + sem (WT Vehicle, $n = 20$; R6/2 Vehicle, $n = 17$; R6/2 30 mg/kg CHDI-340246, $n = 17$; R6/2 60 mg/kg CHDI-00340246, $n = 20$; R6/2100 mg/kg CHDI-00340246, $n = 18$). No significant changes were observed by MRI in (**A**) whole brain volume, (B) striatal volume, or (C) cortical volume after chronic dosing of CHDI-340246. Volumetric changes between WT and R6/2 mice were highly significant (****, $p < 0.0001$); ns = not significant; One Way ANOVA, Tukey's post-hoc multiple comparison test. (D) *in vivo* MR spectroscopy analysis of striatal metabolites. Data are presented as mean ± sem. Changes between WT and R6/2 mice were highly significant (#, $p < 0.001$; *, $p < 0.05$; One Way ANOVA, Tukey's post-hoc multiple comparison test). Only Creatine levels were normalized towards WT at the highest dose of CHDI-340246 dosing ($, $p < 0.05$; One Way ANOVA, Tukey's post-hoc multiple comparison test). Abbreviations: Cr, Creatine; PCr, Phosphocreatine; GABA, Gamma-Aminobutryic Acid; GLN, Glutamine; GLU, Glutamate; GPC, Glycerophosphocholine; PCh, Phosphocholine; GSH, Glutathione; INS, Myo-inositol; NAA, *N*-acetyl-aspartate; TAU, Taurine; CHO, Choline; NAA + NAAG, *N*-acetyl-aspartate and *N*-acetyl-aspartate glutamate; CR + PCr, Creatine + Phosphocreatine.

in the same cohort of animals used for behavioral testing. For the R6/2 study, 12 week old mice were subjected to *in vivo* T2-MRI analysis of total brain, striatum and cortical volumes, and also to 1H-MR Spectroscopy analysis of striatal metabolites including *N*-acetyl-aspartate (NAA), Choline (Cho), Taurine (Tau) and Glutamine (Gln). This type of analyses reveals a significant loss of volume in these structures (Heikkinen et al., 2012). We failed to detect any effect of CHDI-340246 in either male or female mice with the exception of a change in Cretaine (Cr) levels in R6/2 animals treated with 100 mg/kg of CHDI-340246 (Fig. 10). An overall similar lack of volumetric/structural effects was obtained in the Q175 homs study (Fig. S8; measurements conducted at baseline and at 4 and 8 months of age). Additionally, CHDI-340246 had no effect on gene expression changes associated with disease progression in these models, or on soluble levels of HTT protein (data not shown). An RNAseq analysis of striatal gene expression in R6/2 mice chronically dosed with 30 mg/kg CHDI-340246 also revealed no changes in gene expression in the treated mice, suggesting that the modulation of KMO activity does not lead to significant transcriptional changes *in vivo* (data not shown).

4. Discussion

Dysregulation of KP enzymes has been implicated in a variety of conditions, and changing levels of various neuroactive KP metabolites have been correlated with alterations in brain function in the context of affective disorders, cognition, neuroinflammatory disorders and neurodegeneration (Campbell et al., 2014; Maddison and Giorgini, 2015; Stone and Darlington, 2013). Evidence of the KP's involvement largely comes from animal models and humans, but few studies have been conducted with optimized molecules with suitable properties for long-term dosing, a necessary step to evaluate the contribution of specific enzymes to disease progression (Justinova et al., 2013; Kozak et al., 2014).

In this report, we describe the pharmacological properties of a novel, potent and selective KMO inhibitor suitable for chronic dosing studies in preclinical species. We show that CHDI-340246 dose-dependently modulates KMO activity in various tissues. Oral administration with CHDI-340246 resulted in an increase in the levels of Kyn, KynA, and AA in the interstitial fluid and tissues (brain, liver, and kidney), whilst reducing the levels of 3-OH-Kyn in plasma and peripheral tissues. Levels of 3-OH-Kyn were slightly elevated in the brain although CHDI-340246 concentrations exceed the IC_{50} concentrations of KMO at higher doses. This effect is consistent with the contribution of peripheral Kyn penetrating the BBB to the formation of 3-OH-Kyn. Data from treatment with a combination of Kyn and CHDI-340246 are, however, suggestive of an inhibition of KMO expressed inside the CNS by CHDI-340246. Given these properties, and the fact that CHDI-340246 is well tolerated in chronic dosing studies in mice (this study), rats (Toledo-Sherman et al., 2015) and primates (not shown), we consider that CHDI-340246 can help answer fundamental questions about the biology of KMO and the KP in a variety of conditions.

Using CHDI-340246 we describe an extensive set of studies trying to address the relevance of KMO activity in the context of HD mouse models, and the effects of modulation of KP pathway metabolism. Previous reports showed in HD patients (albeit with a small sample size using post-mortem tissues or CSF samples) and in several mouse models of HD, alterations in the KP; most consistently an early elevation

of 3-OH-Kyn levels in the brain (Guidetti et al., 2006; Guidetti et al., 2004; Guidetti et al., 2000; Mazarei et al., 2013; Pearson and Reynolds, 1992; Sathyasaikumar et al., 2010). Although we verified that the activity of KMO is elevated in the striatum of symptomatic Q175 het mice in enzymatic assays conducted with striatal mitochondria isolates, levels of 3-OH-Kyn and Quin are not greatly elevated in the extracellular space, so the biological significance of this seems minimal.

We investigated the role of Kyn, KynA and AA in several synaptic alterations associated with HD, given the neuroactive role ascribed to KynA previously. HD model mice display a deficit in long term plasticity in the hippocampus (R6/2) and neuronal abnormalities in the striatum (R6/2 and Q175). We found that these deficits can be reversed acutely by Kyn, KynA, and various KMO inhibitors at nM concentrations, suggesting a beneficial role for increases in these metabolites in the context of HD synaptic alterations. However, our results do not support that the effect of KynA is mediated via an action on NMDA or α7-nAchR receptors: we show that KP metabolites do not have any significant direct effects on various ionotropic receptors at the concentrations tested in the present study. In our assays, none of the KP metabolites acted as agonists at either the glycine or glutamate site of NMDA receptors at the concentrations tested (up to 300 μM) in heterologous systems. This does not rule out a possible effect at higher Quin concentrations, which might rise dramatically in certain neuro-inflammatory conditions (Heyes et al., 2001; Valle et al., 2004). In the HD models evaluated we showed that interstitial and tissue levels of Quin do not reach levels shown to be neurotoxic, but this does not rule out the possibility that synaptic levels and levels in human disease may be sufficiently high to engage these receptors.

Among the KP metabolites investigated, only KynA can act as an antagonist at both NR2A- and NR2B-containing NMDARs. This is in agreement with published findings that KynA blocks NMDA receptors with preference for NR2A over NR2B-receptors. The KynA concentration in whole brain tissues is reported to be in the range of 0.2-1μM (Moroni et al., 1988; Turski et al., 1988), much lower than the NMDA receptor IC_{50} reported in recombinant cell lines and cultured hippocampal neurons (8–65 μM) (Mok et al., 2009; Parsons et al., 1997). In our hands, the basal extracellular concentrations of KynA in dialysates were in the low nM range, and the levels obtained after CHDI-340246 administration in mice (Table S2) do not reach concentrations sufficient to directly modulate NMDAR complexes.

Similarly, we could also not detect a direct inhibition of α7 nAChR currents by KP metabolites in either patch-clamp or ligand binding competition experiments, which is in agreement with data obtained with recombinant receptors expressed in GH4 cell line and native α7 nAChR in rat cultured hippocampal neurons. (Mok et al., 2009). This contradicts previous findings (Albuquerque and Schwarcz, 2013; Banerjee et al., 2012; Beggiato et al., 2013; Hilmas et al., 2001; Wu et al., 2010), showing that KynA inhibits α7 nAChR ($IC_{50} = 7$ μM) and modulates its signaling. Based on these studies it has been suggested that at physiologically relevant concentrations, KynA exerts a neuroprotective action via nicotinic receptor modulation, rather than on NMDARs. It has been proposed that attenuation of glutamatergic function *in vivo* by KynA (Konradsson-Geuken et al., 2010; Pellicciari et al., 1994) is the result of direct α7 nAChR modulation. However, we and others (Dobelis et al., 2012; Mok et al., 2009; Priestley et al., 1995) could not detect any direct inhibitory effects on α7 nAChR currents.

In the course of our studies, we uncovered a novel role for KMO, and for Kyn/KynA, in the regulation of hippocampal and striatal synaptic and neuronal functioning. The sufficiency of exogenous exposure to Kyn and KynA and their role in the modulation of potassium conductances in SPNs is a novel finding. The rapid and robust effect of nM levels of these metabolites in acute slice preparations suggests that these metabolites exert their action via a high affinity target, whether at the membrane or intracellularly. These metabolites are transported into cells via amino acid transporters, so an intracellular site of action is possible. Therefore, the *direct* mechanism of action of Kyn and KynA in the brain remains unresolved and represents an area of high interest. These observations highlight, however, a potential important role for Kyn itself as a neuroactive molecule, possibly via its role (as described in the vascular endothelium) as a modulator of nitric oxide signaling and regulator of cGMP signaling (Wang et al., 2010).

With regard to HD, the main hypothesis driving our study was the association of elevated KMO activity, and 3-OH-Kyn and Quin levels, with neurodegeneration and neuro-inflammation. Despite elevated KMO activity in the striatum of various mouse models of HD, clearly the levels of 3-OH-Kyn and Quin do not reach levels previously associated with neurotoxicity; this is consistent with HD mouse models not displaying obvious signs of neuronal degeneration or classical neuroinflammation (Heikkinen et al., 2012; Tong et al., 2014). Therefore we cannot ascertain the contribution of classical neuro-inflammatory mechanisms to disease progression in existing genetic models of HD. The only marker of inflammation we routinely use for drug screening is an elevation in TSPO expression, a marker associated with activated microglia (Chen and Guilarte, 2008). In a radioligand binding assay for TSPO, chronic dosing of CHDI-340246 did not reduce TSPO levels in R6/2 mice (not shown). In this study, we did not monitor Iba1 or CD68 expression by immunohistochemistry in striatal tissues, so our data cannot be directly compared to the effects reported for the chronic dosing of JM6 (Zwilling et al., 2011). JM6, a putative precursor to a well-characterized KMO inhibitor, Ro-61-8048 (Rover et al., 1997), was shown to modify disease progression in HD and AD mouse models. We previously reported (Beconi et al., 2012) that JM6 is a very weak KMO inhibitor (μM in biochemical assays with mitochondrial fractions containing KMO, and inactive in cellular assays), and that it did not act as a precursor for Ro-61-8048 (Beconi et al., 2012). Therefore, we questioned the interpretation of this work in terms of linking modulation of KMO activity as the drug's mechanism of action.

Taken together, we show that the 'long term' effects of chronic KMO inhibition in HD mouse models are limited to a potential role in preventing glutamatergic signaling deficits to the striatum, based on the results obtained in the mini EPSC analyses after chronic dosing in both HD mouse models. It is noteworthy that a similar rescue of mEPSC frequency deficits has also been demonstrated following chronic dosing of Q175 hets in the same format using a PDE9 inhibitor (see http://chdifoundation.org/2012-conference-2/#beaumont), again supporting the idea that neurophysiological effects following KMO inhibition look strikingly similar to another strategy that selectively elevates a distinct pool of intracellular cGMP. The link in this case is more correlative / speculative than the work we performed on SPN excitability changes, where CHDI-340246-mediated improvements in HD SPN excitability were shown to be partially mitigated by GC and PKG inhibition. Clearly, further work will need to be performed to strengthen these observations to unambiguously identify common mechanisms responsible for the improvement. In this respect, we attempted to directly measure cyclic nucleotide elevation following whole slice incubations with CHDI-340246 and in the striatum of mice after acute dosing with CHDI-340246, and we could not detect any changes in cAMP or cGMP levels (not shown). However, this does not preclude a potential spatially restricted elevation of cyclic nucleotides after KMO inhibition which would be below the level of detection.

Other classical measurements of disease progression (locomotor, volumetric, molecular, survival), with the exception of an effect in lifespan in male R6/2 mice, did not show any effect of chronic KMO inhibition. In this paper, we did not address any potential effects of CHDI-340246 on cognitive deficits associated with the HD mouse models, although studies in rats did not suggest any benefit of chronic KMO inhibition on a variety of tasks in wildtype animals (not shown). Of interest, previous reports have shown a potential detrimental effect of systemic administration of Kyn and of elevated KynA in various locomotor and

cognitive tasks (Kozak et al., 2014; Varga et al., 2015). We did not observe any detrimental effects of CHDI-340246 in open field tests, rearing tests, rotarod, or in neurological scores, in spite of elevating KynA levels significantly in the brain. The reason for this discrepancy is unclear but could suggest that elevations of Kyn/KynA via KMO inhibition might lead to different effects from those observed with either direct Kyn administration (which profoundly elevates 3-OH-Kyn and Quin in tissues and plasma) or via the inhibition of KAT activity (Kozak et al., 2014). Collectively, our findings contrast with those reported by Zwilling et al. (Zwilling et al., 2011), and do not support a significant role for peripheral KMO inhibition in disease progression measures in HD mouse models.

Despite our findings using these HD models, many studies have shown a strong correlation between IDO (indoleamine 2,3-dioxygenase, a key enzyme responsible for the production of kynurenine from tryptophan) activation, in situ-generated Quin neurotoxic levels, and the extent of neurodegeneration (Kandanearatchi and Brew, 2012; Plangar et al., 2012; Stone and Darlington, 2013; Vamos et al., 2009). The role of kynurenine catabolism in the regulation of the immune response is important, and this is difficult to evaluate in mouse models of HD. We therefore consider that the role of Quin elevation and dysregulation of KMO activity in neurodegeneration and neuro-inflammation is worth testing in conditions displaying significant neuronal cell loss and glial activation, including in HD patients (Crotti and Glass, 2015; Tai et al., 2007; Waldvogel et al., 2015). We are in the process of independently assessing whether levels of KP metabolites are altered in the CSF of clinically well-characterized HD patients. CHDI-340246 can potently inhibit KMO both inside and outside the CNS in a dose-dependent manner, and could be used, pending safety data in humans, to assess the contribution of this catabolic branch of the kynurenine pathway to neurodegenerative and inflammatory conditions.

Supplementary data to this article can be found online at http://dx.doi.org/10.1016/j.expneurol.2016.05.005.

Funding disclosure

All studies were funded by CHDI Foundation. CHDI Foundation is a privately-funded nonprofit biomedical research organization exclusively dedicated to discovering and developing therapeutics that slow the progression of Huntington's disease. CHDI Foundation conducts research in a number of different ways; for the purposes of this manuscript, research was conducted at the contract research organizations Evotec, Neuroservice, Psychogenics, Brains Online and Charles River (Finland) under fee-for-service agreements.

Competing interests

The authors have declared that no competing interests exist. VB, LM, IM-S, LP, LT-S, VK and CD are employed by CHDI Management, Inc., as advisors to CHDI Foundation, Inc. These authors contributed to the conception, planning, and direction of the research, including analysis and interpretation of the data. For the purposes of this manuscript, all non-CHDI Foundation authors conducted work strictly as fee-per-service on behalf of CHDI Foundation. CHDI-340246 is claimed in patent WO 2013033085 *A*1, owned by CHDI Foundation, Inc.

Author contributions

VB, LM, IM-S, LP, LT-S, VK and CD all participated in the experimental design and data analysis. VB and IMS wrote the paper, VB coordinated all electrophysiology experiments at PGI and Neuroservice. ES, MG (hippocampal MEA), GT, SG and AB (SPN and corticostriatal evaluation) conducted the electrophysiology experiments reported. RJ provided electrophysiology analysis support and draft compilation of manuscript. IM-S and LM coordinated all microdialysis experiments at Brains Online. UD, RF, MH and AR conducted all the microdialysis experiments and data analysis of pharmacodynamics effects. VK and CD coordinated all pharmacokinetic experiments. LP coordinated all *in vivo* efficacy testing in HD rodent models reported. TH, KL, JP, and OK conducted all *in vivo* HD rodent model testing of CHDI-340246. LT-S, LM, IM-S and CD coordinated all studies leading to the development of CHDI-340246 at Evotec. IN, HD, DW, and AE conducted all studies at Evotec.

Acknowledgments

We would like to acknowledge comments to the manuscript by Simon Noble, Bernhard Landwehrmeyer and Steve Goldman.

References

Albuquerque, E.X., Schwarcz, R., 2013. Kynurenic acid as an antagonist of alpha7 nicotinic acetylcholine receptors in the brain: facts and challenges. Biochem. Pharmacol. 85, 1027–1032.
Amaral, M., Levy, C., Heyes, D.J., Lafite, P., Outeiro, T.F., Giorgini, F., Leys, D., Scrutton, N.S., 2013. Structural basis of kynurenine 3-monooxygenase inhibition. Nature 496, 382–385.
Amori, L., Guidetti, P., Pellicciari, R., Kajii, Y., Schwarcz, R., 2009. On the relationship between the two branches of the kynurenine pathway in the rat brain in vivo. J. Neurochem. 109, 316–325.
Ariano, M.A., Cepeda, C., Calvert, C.R., Flores-Hernandez, J., Hernandez-Echeagaray, E., Klapstein, G.J., Chandler, S.H., Aronin, N., DiFiglia, M., Levine, M.S., 2005. Striatal potassium channel dysfunction in Huntington's disease transgenic mice. J. Neurophysiol. 93, 2565–2574.
Banerjee, J., Alkondon, M., Albuquerque, E.X., 2012. Kynurenic acid inhibits glutamatergic transmission to CA1 pyramidal neurons via alpha7 nAChR-dependent and -independent mechanisms. Biochem. Pharmacol. 84, 1078–1087.
Beal, M.F., Ferrante, R.J., Swartz, K.J., Kowall, N.W., 1991. Chronic quinolinic acid lesions in rats closely resemble Huntington's disease. J. Neurosci. 11, 1649–1659.
Beaumont, V., Park, L., Rassoulpour, A., Dijkman, U., Heikkinen, T., Lehtimaki, K., Kontkanen, O., Al Nackkash, R., Bates, G.P., Gleyzes, M., Steidl, E., Ramboz, S., Murphy, C., Beconi, M.G., Dominguez, C., Munoz-Sanjuan, I., 2014. The PDE1/5 inhibitor SCH-51866 does not modify disease progression in the R6/2 mouse model of Huntington's disease. PLoS currents 6.
Beconi, M.G., Yates, D., Lyons, K., Matthews, K., Clifton, S., Mead, T., Prime, M., Winkler, D., O'Connell, C., Walter, D., Toledo-Sherman, L., Munoz-Sanjuan, I., Dominguez, C., 2012. Metabolism and pharmacokinetics of JM6 in mice: JM6 is not a prodrug for Ro-61-8048. Drug Metab. Dispos. 40, 2297–2306.
Beggiato, S., Antonelli, T., Tomasini, M.C., Tanganelli, S., Fuxe, K., Schwarcz, R., Ferraro, L., 2013. Kynurenic acid, by targeting alpha7 nicotinic acetylcholine receptors, modulates extracellular GABA levels in the rat striatum in vivo. Eur. J. Neurosci. 37, 1470–1477.
Campbell, B.M., Charych, E., Lee, A.W., Moller, T., 2014. Kynurenines in CNS disease: Regulation by inflammatory cytokines. Front. Neurosci. 8, 12.
Campesan, S., Green, E.W., Breda, C., Sathyasaikumar, K.V., Muchowski, P.J., Schwarcz, R., Kyriacou, C.P., Giorgini, F., 2011. The kynurenine pathway modulates neurodegeneration in a drosophila model of Huntington's disease. Curr. Biol. 21, 961–966.
Cepeda, C., Hurst, R.S., Calvert, C.R., Hernandez-Echeagaray, E., Nguyen, O.K., Jocoy, E., Christian, L.J., Ariano, M.A., Levine, M.S., 2003. Transient and progressive electrophysiological alterations in the corticostriatal pathway in a mouse model of Huntington's disease. J. Neurosci. 23, 961–969.
Cepeda, C., Galvan, L., Holley, S.M., Rao, S.P., Andre, V.M., Botelho, E.P., Chen, J.Y., Watson, J.B., Deisseroth, K., Levine, M.S., 2013. Multiple sources of striatal inhibition are differentially affected in huntington's disease mouse models. J. Neurosci. 33 (17), 7393–7406.
Chen, M.K., Guilarte, T.R., 2008. Translocator protein 18 kDa (TSPO): molecular sensor of brain injury and repair. Pharmacol. Ther. 118, 1–17.
Connick, J.H., Stone, T.W., Carla, V., Moroni, F., 1988. Increased kynurenic acid levels in Huntington's disease. Lancet 2, 1373.
Cowan, C.M., Raymond, L.A., 2006. Selective neuronal degeneration in Huntington's disease. Curr. Top. Dev. Biol. 75, 25–71.
Crotti, A., Glass, C.K., 2015. The choreography of neuroinflammation in Huntington's disease. Trends Immunol. 36, 364–373.
Dobelis, P., Staley, K.J., Cooper, D.C., 2012. Lack of modulation of nicotinic acetylcholine alpha-7 receptor currents by kynurenic acid in adult hippocampal interneurons. PLoS One 7, e41108.
Ferrante, R.J., Kowall, N.W., Cipolloni, P.B., Storey, E., Beal, M.F., 1993. Excitotoxin lesions in primates as a model for Huntington's disease: histopathologic and neurochemical characterization. Exp. Neurol. 119, 46–71.
Forrest, C.M., Mackay, G.M., Stoy, N., Spiden, S.L., Taylor, R., Stone, T.W., Darlington, L.G., 2010. Blood levels of kynurenines, interleukin-23 and soluble human leucocyte antigen-G at different stages of Huntington's disease. J. Neurochem. 112, 112–122.
Foster, A.C., Kemp, J.A., Leeson, P.D., Grimwood, S., Donald, A.E., Marshall, G.R., Priestley, T., Smith, J.D., Carling, R.W., 1992. Kynurenic acid analogues with improved affinity and selectivity for the glycine site on the *N*-methyl-D-aspartate receptor from rat brain. Mol. Pharmacol. 41, 914–922.
Fukui, S., Schwarcz, R., Rapoport, S.I., Takada, Y., Smith, Q.R., 1991. Blood-brain barrier transport of kynurenines: implications for brain synthesis and metabolism. J. Neurochem. 56, 2007–2017.

Giorgini, F., Huang, S.Y., Sathyasaikumar, K.V., Notarangelo, F.M., Thomas, M.A., Tararina, M., Wu, H.Q., Schwarcz, R., Muchowski, P.J., 2013. Targeted deletion of kynurenine 3-monooxygenase in mice: a new tool for studying kynurenine pathway metabolism in periphery and brain. J. Biol. Chem. 288, 36554–36566.

Graham, R.K., Pouladi, M.A., Joshi, P., Lu, G., Deng, Y., Wu, N.P., Figueroa, B.E., Metzler, M., Andre, V.M., Slow, E.J., Raymond, L., Friedlander, R., Levine, M.S., Leavitt, B.R., Hayden, M.R., 2009. Differential susceptibility to excitotoxic stress in YAC128 mouse models of Huntington disease between initiation and progression of disease. J. Neurosci. 29, 2193–2204.

Guidetti, P., Reddy, P.H., Tagle, D.A., Schwarcz, R., 2000. Early kynurenergic impairment in Huntington's disease and in a transgenic animal model. Neurosci. Lett. 283, 233–235.

Guidetti, P., Luthi-Carter, R.E., Augood, S.J., Schwarcz, R., 2004. Neostriatal and cortical quinolinate levels are increased in early grade Huntington's disease. Neurobiol. Dis. 17, 455–461.

Guidetti, P., Bates, G.P., Graham, R.K., Hayden, M.R., Leavitt, B.R., MacDonald, M.E., Slow, E.J., Wheeler, V.C., Woodman, B., Schwarcz, R., 2006. Elevated brain 3-hydroxykynurenine and quinolinate levels in Huntington disease mice. Neurobiol. Dis. 23, 190–197.

Hansson, O., Petersen, A., Leist, M., Nicotera, P., Castilho, R.F., Brundin, P., 1999. Transgenic mice expressing a Huntington's disease mutation are resistant to quinolinic acid-induced striatal excitotoxicity. Proc. Natl. Acad. Sci. U. S. A. 96, 8727–8732.

Hansson, O., Guatteo, E., Mercuri, N.B., Bernardi, G., Li, X.J., Castilho, R.F., Brundin, P., 2001. Resistance to NMDA toxicity correlates with appearance of nuclear inclusions, behavioural deficits and changes in calcium homeostasis in mice transgenic for exon 1 of the Huntington gene. Eur. J. Neurosci. 14, 1492–1504.

Heikkinen, T., Lehtimaki, K., Vartiainen, N., Puolivali, J., Hendricks, S.J., Glaser, J.R., Bradaia, A., Wadel, K., Touller, C., Kontkanen, O., Yrjanheikki, J.M., Buisson, B., Howland, D., Beaumont, V., Munoz-Sanjuan, I., Park, L.C., 2012. Characterization of neurophysiological and behavioral changes, MRI brain volumetry and 1H MRS in zQ175 knock-in mouse model of Huntington's disease. PLoS One 7, e50717.

Heyes, M.P., Morrison, P.F., 1997. Quantification of local de novo synthesis versus blood contributions to quinolinic acid concentrations in brain and systemic tissues. J. Neurochem. 68, 280–288.

Heyes, M.P., Ellis, R.J., Ryan, L., Childers, M.E., Grant, I., Wolfson, T., Archibald, S., Jernigan, T.L., Center, H.G.H.N.R., 2001. Elevated cerebrospinal fluid quinolinic acid levels are associated with region-specific cerebral volume loss in HIV infection. Brain 124, 1033–1042.

Heyes, M.P., Chen, C.Y., Major, E.O., Saito, K., 1997. Different kynurenine pathway enzymes limit quinolinic acid formation by various human cell types. Biochem. J. 326 (Pt 2), 351–356.

Hilmas, C., Pereira, E.F., Alkondon, M., Rassoulpour, A., Schwarcz, R., Albuquerque, E.X., 2001. The brain metabolite kynurenic acid inhibits alpha7 nicotinic receptor activity and increases non-alpha7 nicotinic receptor expression: physiopathological implications. J. Neurosci. 21, 7463–7473.

Jauch, D.A., Sethy, V.H., Weick, B.G., Chase, T.N., Schwarcz, R., 1993. Intravenous administration of L-kynurenine to rhesus monkeys: Effect on quinolinate and kynurenate levels in serum and cerebrospinal fluid. Neuropharmacology 32, 467–472.

Justinova, Z., Mascia, P., Wu, H.Q., Secci, M.E., Redhi, G.H., Panlilio, L.V., Scherma, M., Barnes, C., Parashos, A., Zara, T., Fratta, W., Solinas, M., Pistis, M., Bergman, J., Kangas, B.D., Ferre, S., Tanda, G., Schwarcz, R., Goldberg, S.R., 2013. Reducing cannabinoid abuse and preventing relapse by enhancing endogenous brain levels of kynurenic acid. Nat. Neurosci. 16, 1652–1661.

Kandanearatchi, A., Brew, B.J., 2012. The kynurenine pathway and quinolinic acid: pivotal roles in HIV associated neurocognitive disorders. FEBS J 279, 1366–1374.

Kessler, M., Terramani, T., Lynch, G., Baudry, M., 1989. A glycine site associated with N-methyl-D-aspartic acid receptors: characterization and identification of a new class of antagonists. J. Neurochem. 52, 1319–1328.

Kita, T., Morrison, P.F., Heyes, M.P., Markey, S.P., 2002. Effects of systemic and central nervous system localized inflammation on the contributions of metabolic precursors to the L-kynurenine and quinolinic acid pools in brain. J. Neurochem. 82, 258–268.

Konradsson-Geuken, A., Wu, H.Q., Gash, C.R., Alexander, K.S., Campbell, A., Sozeri, Y., Pellicciari, R., Schwarcz, R., Bruno, J.P., 2010. Cortical kynurenic acid bi-directionally modulates prefrontal glutamate levels as assessed by microdialysis and rapid electrochemistry. Neuroscience 169, 1848–1859.

Kozak, R., Campbell, B.M., Strick, C.A., Horner, W., Hoffmann, W.E., Kiss, T., Chapin, D.S., McGinnis, D., Abbott, A.L., Roberts, B.M., Fonseca, K., Guanowsky, V., Young, D.A., Seymour, P.A., Dounay, A., Hajos, M., Williams, G.V., Castner, S.A., 2014. Reduction of brain kynurenic acid improves cognitive function. J. Neurosci. 34, 10592–10602.

Maddison, D.C., Giorgini, F., 2015. The kynurenine pathway and neurodegenerative disease. Semin. Cell Dev. Biol. 40, 134–141.

Mangiarini, L., Sathasivam, K., Seller, M., Cozens, B., Harper, A., Hetherington, C., Lawton, M., Trottier, Y., Lehrach, H., Davies, S.W., Bates, G.P., 1996. Exon 1 of the HD gene with an expanded CAG repeat is sufficient to cause a progressive neurological phenotype in transgenic mice. Cell 87, 493–506.

Mazarei, G., Budac, D.P., Lu, G., Adomat, H., Tomlinson Guns, E.S., Moller, T., Leavitt, B.R., 2013. Age-dependent alterations of the kynurenine pathway in the YAC128 mouse model of Huntington disease. J. Neurochem. 127, 852–867.

Menalled, L.B., Kudwa, A.E., Miller, S., Fitzpatrick, J., Watson-Johnson, J., Keating, N., Ruiz, M., Mushlin, R., Alosio, W., McConnell, K., Connor, D., Murphy, C., Oakeshott, S., Kwan, M., Beltran, J., Ghavami, A., Brunner, D., Park, L.C., Ramboz, S., Howland, D., 2012. Comprehensive behavioral and molecular characterization of a new knock-in mouse model of Huntington's disease: zQ175. PLoS One 7, e49838.

Mielcarek, M., Landles, C., Weiss, A., Bradaia, A., Seredenina, T., Inuabasi, L., Osborne, G.F., Wadel, K., Touller, C., Butler, R., Robertson, J., Franklin, S.A., Smith, D.L., Park, L., Marks, P.A., Wanker, E.E., Olson, E.N., Luthi-Carter, R., van der Putten, H., Beaumont, V., Bates, G.P., 2013. HDAC4 reduction: a novel therapeutic strategy to target cytoplasmic huntingtin and ameliorate neurodegeneration. PLoS Biol. 11, e1001717.

Mok, M.H., Fricker, A.C., Weil, A., Kew, J.N., 2009. Electrophysiological characterisation of the actions of kynurenic acid at ligand-gated ion channels. Neuropharmacology 57, 242–249.

Monaghan, D.T., Beaton, J.A., 1991. Quinolinate differentiates between forebrain and cerebellar NMDA receptors. Eur. J. Pharmacol. 194, 123–125.

Moroni, F., Russi, P., Lombardi, G., Beni, M., Carla, V., 1988. Presence of kynurenic acid in the mammalian brain. J. Neurochem. 51, 177–180.

Moroni, F., Cozzi, A., Carpendo, R., Cipriani, G., Veneroni, O., Izzo, E., 2005. Kynurenine 3-mono-oxygenase inhibitors reduce glutamate concentration in the extracellular spaces of the basal ganglia but not in those of the cortex or hippocampus. Neuropharmacology 48, 788–795.

Murphy, K.P., Carter, R.J., Lione, L.A., Mangiarini, L., Mahal, A., Bates, G.P., Dunnett, S.B., Morton, A.J., 2000. Abnormal synaptic plasticity and impaired spatial cognition in mice transgenic for exon 1 of the human Huntington's disease mutation. J. Neurosci. 20, 5115–5123.

Parsons, C.G., Danysz, W., Quack, G., Hartmann, S., Lorenz, B., Wollenburg, C., Baran, L., Przegalinski, E., Kostowski, W., Krzascik, P., Chizh, B., Headley, P.M., 1997. Novel systemically active antagonists of the glycine site of the N-methyl-D-aspartate receptor: electrophysiological, biochemical and behavioral characterization. J. Pharmacol. Exp. Ther. 283, 1264–1275.

Pearson, S.J., Reynolds, G.P., 1992. Increased brain concentrations of a neurotoxin, 3-hydroxykynurenine, in Huntington's disease. Neurosci. Lett. 144, 199–201.

Pellicciari, R., Natalini, B., Costantino, G., Mahmoud, M.R., Mattoli, L., Sadeghpour, B.M., Moroni, F., Chiarugi, A., Carpenedo, R., 1994. Modulation of the kynurenine pathway in search for new neuroprotective agents. Synthesis and preliminary evaluation of (m-nitrobenzoyl)alanine, a potent inhibitor of kynurenine-3-hydroxylase. J. Med. Chem. 37, 647–655.

Petersen, A., Chase, K., Puschban, Z., DiFiglia, M., Brundin, P., Aronin, N., 2002. Maintenance of susceptibility to neurodegeneration following intrastriatal injections of quinolinic acid in a new transgenic mouse model of Huntington's disease. Exp. Neurol. 175, 297–300.

Plangar, I., Majlath, Z., Vecsei, L., 2012. Kynurenines in cognitive functions: their possible role in depression. Neuropsychopharmacol Hung 14, 239–244.

Priestley, T., Laughton, P., Myers, J., Le, B.B., Kerby, J., Whiting, P.J., 1995. Pharmacological properties of recombinant human N-methyl-D-aspartate receptors comprising NR1a/NR2A and NR1a/NR2B subunit assemblies expressed in permanently transfected mouse fibroblast cells. Mol. Pharmacol. 48, 841–848.

Ross, C.A., Aylward, E.H., Wild, E.J., Langbehn, D.R., Long, J.D., Warner, J.H., Scahill, R.I., Leavitt, B.R., Stout, J.C., Paulsen, J.S., Reilmann, R., Unschuld, P.G., Wexler, A., Margolis, R.L., Tabrizi, S.J., 2014. Huntington disease: natural history, biomarkers and prospects for therapeutics. Nat. Rev. Neurol. 10, 204–216.

Rover, S., Cesura, A.M., Huguenin, P., Kettler, R., Szente, A., 1997. Synthesis and biochemical evaluation of N-(4-phenylthiazol-2-yl)benzenesulfonamides as high-affinity inhibitors of kynurenine 3-hydroxylase. J. Med. Chem. 40, 4378–4385.

Sathyasaikumar, K.V., Stachowski, E.K., Amori, L., Guidetti, P., Muchowski, P.J., Schwarcz, R., 2010. Dysfunctional kynurenine pathway metabolism in the R6/2 mouse model of Huntington's disease. J. Neurochem. 113, 1416–1425.

Schwarcz, R., Guidetti, P., Sathyasaikumar, K.V., Muchowski, P.J., 2010. Of mice, rats and men: revisiting the quinolinic acid hypothesis of Huntington's disease. Prog. Neurobiol. 90, 230–245.

Stone, T.W., Darlington, L.G., 2013. The kynurenine pathway as a therapeutic target in cognitive and neurodegenerative disorders. Br. J. Pharmacol. 169, 1211–1227.

Stoy, N., Mackay, G.M., Forrest, C.M., Christofides, J., Egerton, M., Stone, T.W., Darlington, L.G., 2005. Tryptophan metabolism and oxidative stress in patients with Huntington's disease. J. Neurochem. 93, 611–623.

Tai, Y.F., Pavese, N., Gerhard, A., Tabrizi, S.J., Barker, R.A., Brooks, D.J., Piccini, P., 2007. Imaging microglial activation in Huntington's disease. Brain Res. Bull. 72, 148–151.

The Huntington's Disease Collaborative Research Group, 1993. A novel gene containing a trinucleotide repeat that is expanded and unstable on Huntington's disease chromosomes. The Huntington's disease collaborative research group. Cell 72, 971–983.

Toledo-Sherman, L.M., Prime, M.E., Mrzljak, L., Beconi, M.G., Beresford, A., Brookfield, F.A., Brown, C.J., Cardaun, I., Courtney, S.M., Dijkman, U., Hamelin-Flegg, E., Johnson, P.D., Kempf, V., Lyons, K., Matthews, K., Mitchell, W.L., O'Connell, C., Pena, P., Powell, K., Rassoulpour, A., Reed, L., Reindl, W., Selvaratnam, S., Friley, W.W., Weddell, D.A., Went, N.E., Wheelan, P., Winkler, C., Winkler, D., Wityak, J., Yarnold, C.J., Yates, D., Munoz-Sanjuan, I., Dominguez, C., 2015. Development of a series of aryl pyrimidine kynurenine monooxygenase inhibitors as potential therapeutic agents for the treatment of Huntington's disease. J. Med. Chem. 58, 1159–1183.

Tong, X., Ao, Y., Faas, G.C., Nwaobi, S.E., Xu, J., Haustein, M.D., Anderson, M.A., Mody, I., Olsen, M.L., Sofroniew, M.V., Khakh, B.S., 2014. Astrocyte Kir4.1 ion channel deficits contribute to neuronal dysfunction in Huntington's disease model mice. Nat. Neurosci. 17, 694–703.

Turski, W.A., Nakamura, M., Todd, W.P., Carpenter, B.K., Whetsell Jr., W.O., Schwarcz, R., 1988. Identification and quantification of kynurenic acid in human brain tissue. Brain Res. 454, 164–169.

Valle, M., Price, R.W., Nilsson, A., Heyes, M., Verotta, D., 2004. CSF quinolinic acid levels are determined by local HIV infection: cross-sectional analysis and modelling of dynamics following antiretroviral therapy. Brain 127, 1047–1060.

Vamos, E., Pardutz, A., Klivenyi, P., Toldi, J., Vecsei, L., 2009. The role of kynurenines in disorders of the central nervous system: possibilities for neuroprotection. J. Neurol. Sci. 283, 21–27.

Varga, D., Heredi, J., Kanvasi, Z., Ruszka, M., Kis, Z., Ono, E., Iwamori, N., Iwamori, T., Takakuwa, H., Vecsei, L., Toldi, J., Gellert, L., 2015. Systemic L-kynurenine sulfate

administration disrupts object recognition memory, alters open field behavior and decreases c-Fos immunopositivity in C57Bl/6 mice. Front. Behav. Neurosci. 9, 157.
Waldvogel, H.J., Kim, E.H., Tippett, L.J., Vonsattel, J.P., Faull, R.L., 2015. The neuropathology of Huntington's disease. Curr. Top. Behav. Neurosci. 22, 33–80.
Wang, Y., Liu, H., McKenzie, G., Witting, P.K., Stasch, J.P., Hahn, M., Changsirivathanathamrong, D., Wu, B.J., Ball, H.J., Thomas, S.R., Kapoor, V., Celermajer, D.S., Mellor, A.L., Keaney Jr., J.F., Hunt, N.H., Stocker, R., 2010. Kynurenine is an endothelium-derived relaxing factor produced during inflammation. Nat. Med. 16, 279–285.
Waters, C.W., Varuzhanyan, G., Talmadge, R.J., Voss, A.A., 2013. Huntington disease skeletal muscle is hyperexcitable owing to chloride and potassium channel dysfunction. Proc. Natl. Acad. Sci. U. S. A. 110, 9160–9165.
Williams, M.E., Burton, B., Urrutia, A., Shcherbatko, A., Chavez-Noriega, L.E., Cohen, C.J., Aiyar, J., 2005. Ric-3 promotes functional expression of the nicotinic acetylcholine receptor alpha7 subunit in mammalian cells. J. Biol. Chem. 280, 1257–1263.
Winkler, D., Beconi, M., Toledo-Sherman, L.M., Prime, M., Ebneth, A., Dominguez, C., Munoz-Sanjuan, I., 2013. Development of LC/MS/MS, high-throughput enzymatic and cellular assays for the characterization of compounds that inhibit kynurenine monooxygenase (KMO). J. Biomol. Screen. 18, 879–889.
Wu, H.Q., Pereira, E.F., Bruno, J.P., Pellicciari, R., Albuquerque, E.X., Schwarcz, R., 2010. The astrocyte-derived alpha7 nicotinic receptor antagonist kynurenic acid controls extracellular glutamate levels in the prefrontal cortex. J. Mol. Neurosci. 40, 204–210.
Zadori, D., Nyiri, G., Szonyi, A., Szatmari, I., Fulop, F., Toldi, J., Freund, T.F., Vecsei, L., Klivenyi, P., 2011. Neuroprotective effects of a novel kynurenic acid analogue in a transgenic mouse model of Huntington's disease. J. Neural Transm. 118, 865–875.
Zwilling, D., Huang, S.Y., Sathyasaikumar, K.V., Notarangelo, F.M., Guidetti, P., Wu, H.Q., Lee, J., Truong, J., Andrews-Zwilling, Y., Hsieh, E.W., Louie, J.Y., Wu, T., Scearce-Levie, K., Patrick, C., Adame, A., Giorgini, F., Moussaoui, S., Laue, G., Rassoulpour, A., Flik, G., Huang, Y., Muchowski, J.M., Masliah, E., Schwarcz, R., Muchowski, P.J., 2011. Kynurenine 3-monooxygenase inhibition in blood ameliorates neurodegeneration. Cell 145, 863–874.